School of Mechanical and
Aerospace Engineering
Ashby Building
Stranmillis Road
Belfast
BT9 5AH

Mechanical and Aerospace Engineering

Project 3 Report

MEE3030

Development of a Battery Management System Protocol to Measure the Condition of an Electric Vehicle Battery

Author N McCleery [40042389]
Project supervisor Dr. A. Foley
Programme BEng Mechanical Engineering
Date 1st April 2014
Report revision 4

Abstract

In a global environment characterised by rising fossil fuel prices and dwindling reserves, where unflinching pressure to reduce harmful emissions shows no sign of abating; the automotive industry is being forced to seek out improved efficiencies and investigate new technologies. This pursuit of increased efficiency has led many vehicle manufacturers to design, manufacture and market battery powered electric vehicles. However, when compared with traditional hydrocarbons, current battery technologies have an inherent specific energy capacity deficit. To mitigate the effects of this energy deficit, efficiency maximising control systems must be applied to electric vehicle battery systems. These battery management systems serve a variety of functions, aiming to maximise available energy capacity, prolong service life and prevent catastrophic failures.

This report documents research undertaken in developing such a battery management system protocol. This protocol has been developed and tested alongside a software based electric vehicle simulation package. Targeting increased battery life and improved efficiency, the described protocol is capable of continually monitoring a battery's state of charge, state of health and delivered energy. It may also record battery charging and discharging times and temperatures. The developed protocol has then been used to monitor and analyse the behaviour of a simulated electric vehicle battery under differing drive cycles. Where possible, these results have then been compared with manufacturer's published specifications.

Acknowledgments

Thanks are extended to Dr. Aoife Foley for her guidance throughout the project. The author also wishes to express his appreciation for the advice offered by Stephen Dillon, Norman Cornett and Gerry Rafferty.

Table of Contents

List of Figures

List of Tables

Nomenclature

Symbols:

a	Acceleration	[m/s^2]
A	area	[m^2]
C	Capacity	[Ah, mAh, C]
$DischargeRates$	Discharge Rates	[dataset]
DOD	Depth of discharge	[%, dimensionless]
$DriveCycle$	Drive cycle	[dataset]
F	Force	[N]
$Height$	Battery pack height	[cells]
I	Current	[A]
K	Coefficient	[dimensionless]
m	Mass	[kg]
P	Power	[W, kW]
r	Ratio	[dimensionless]
SOC	State of charge	[%, dimensionless]
t	Time	[s, h]
T	Temperature	[°C]
V	Voltage	[V]
v	Velocity	[m/s, kph]
$Width$	Battery pack width	[cells]
η	Efficiency	[dimensionless]
τ	Time period	[s, h]

Subscripts:

A	Tyre, coefficient of
$Achiveable$	Maximum achievable (capacity)
B	Tyre, coefficient of
$Balancing$	Balancing condition, property of
$Battery$	Battery property
$BatteryPack$	Battery property, at battery terminals
C	Tyre, coefficient of
Car	Vehicle, property of
CC	Coulomb counting
$Cell$	Cell property, at cell terminals
$Charge$	Charge, charging
$Current$	At a specified time, t
D	Drag, coefficient of
$Demand$	Load, demand, request
$Discharge$	Discharge, discharging
$Drag$	Resistive, in producing drag force
$Drivetrain$	Efficiency, coefficient of
$Frontal$	Front of vehicle, fluid facing
$Initial$	At time t = 0
N	Normal to, reaction
$Parasitic$	Parasitic loss, power
r	Releasable, available
$Rated$	Manufacturer rated (capacity)

Subscripts (cont.):

Terminal	At battery terminals
Tractive	Tractive, in providing tractive force
Voltage	Cell voltage, ratio of
Wheel	At vehicle wheels, power
Wheels	Vehicle wheels, number of

Abbreviations:

ADC	Analogue-to-digital converter
BEV	Battery electric vehicle
BMS	Battery management system
DAQ	Data acquisition
DC	Direct current
DOD	Depth of discharge
DTSC	Dual tiered switched capacitor
EPA	Environmental Protection Agency
EREV	Extended range electric vehicle
HEV	Hybrid electric vehicle
ICE	Internal combustion engine
Li-ion	Lithium-ion
Li-poly	Lithium-polymer
MWT	Multi-windings transformer
NEDC	New European Drive Cycle
Ni-MH	Nickel-metal hydride
OCV	Open circuit voltage
Pb-Acid	Lead-acid
PHEV	Plug-in hybrid electric vehicle
SC	Switched capacitor
SI	Switched inductor
SOC	State of charge
SOH	State of health
SPI	Serial Peripheral Interface
SSC	Single switched capacitor
SWT	Single-winding transformer
UNECE	United Nations Economic Commission for Europe

Definitions:

Concatenation is the 'end-to-end' joining of data.

Electrolyte is a substance containing ions which may be decomposed by application of direct current.

Energy density is energy content per unit mass, or per unit volume, of a fuel or energy storage method.

Hydrolysis refers to the separation of water into its constituent elements, hydrogen and oxygen.

Power density is the power produced per unit mass, or per unit volume, by a battery.

Reversal is the act of applying charge to a battery with the incorrect polarity.

Separator refers to a permeable membrane which permits the flow of charged ions whilst preventing flow of electrons.

1 Introduction

Amidst growing international pressure to reduce potentially harmful emissions and dependence on fossil fuels, several car manufacturers have already brought to market both hybrid electric and fully electric vehicles such as the Toyota Prius [1] and the Mercedes SLS AMG Electric Drive [2]. Considering recent legislation, the Parliamentary Office of Science and Technology [3] state that in 2012, European regulation limiting the average emissions of new cars was first introduced, claiming that this has provided increased financial incentive for manufacturers to develop electric vehicles and electric vehicle technology. Coupled with the UK's 2008 Climate Change Act [4], which stipulates that an 80% reduction in 1990 level greenhouse gas emissions must be achieved by 2050, it seems likely that many manufacturers will thus be left no option but to adopt the technology in the near future, should they wish to continue selling vehicles within the United Kingdom. Unfortunately, whilst contemporary electric vehicles may offer increased efficiency and minimal emissions during use, in many cases their on-board battery technologies are not capable of providing the range or charging times required to draw consumers away from traditional internal combustion engine (ICE) vehicles.

However, when compared with older battery chemistries such as lead-acid and nickel-metal hydride, recently developed chemistries such as lithium-ion and lithium-polymer can yield much improved specific performance and range capability, with further potential for reduced charging times. These more recent lithium based technologies appear to offer fully electric vehicles the potential performance required to make them a viable alternative to internal combustion and hybrid electric vehicles.

Crucially, to try and minimise any adverse effects arising from any specific energy capacity deficit that current battery technologies feature when compared with hydrocarbon fuels, almost all battery types require careful management for electric vehicle application. As a result, a comprehensive battery control system is a necessity for any electric vehicle, helping to increase vehicle performance, range and service life. This system must be capable of monitoring key battery parameters and, if necessary, actively making changes to battery and vehicle operating conditions to ensure that the battery pack is kept within its optimum operating window. It may also be required to report battery status, condition and fault diagnostic information to both the user and other on-board vehicle control systems. This battery management system (BMS) is active during both charging and discharging, optimising battery usage and helping prevent damage.

1.1 Aim of the Research

The project aims to develop a functional and effective battery management system protocol for use with an electric vehicle. Mathematical models of various system components will be created prior to, or in lieu of, the design and manufacture of any hardware required for real-world deployment of the protocol. Where true electric vehicle batteries are not available for design, testing and development of the protocol, mathematical models or replacement units may be used. However, the intention of this project is to produce a complete battery management system protocol that could ultimately be deployed for use in an electric vehicle.

1.2 Structure of the Report

This report contains six chapters and six appendices. In Chapter 1 the topic is introduced. In Chapter 2 current literature and existing technology is reviewed. In Chapter 3 the applied methods for protocol and simulation development are described. In Chapter 4 the design of a prototype is briefly described. In Chapter 5 results are documented and analysed. In Chapters 6 and 7 the results are discussed and the report concluded. Appendix A documents the project management work that has taken place. Appendix B shows some examples of the developed software simulation package's operation and graphical user interface. Appendix C gives a pseudocode version of the final battery management protocol. Appendices D, E and F give full details of the designed prototype. Referencing and style follow IEEE guidelines throughout.

1.3 Limitations

Due to the limited availability of true electric vehicle batteries, mathematical models have been used to enable protocol development. As these mathematical methods are highly dependent on input parameters, simulated behaviour may not be truly representative until all models can be calibrated against real data. Furthermore, all systems have been considered as operating on direct current, with no model for electric motor behaviour included. Elsewhere, vehicle simulation may not fully account for pneumatic tyre behaviour, drag forces and parasitic loads. Beyond model characteristics, further sources of inaccuracy include limited 'drive-cycle' sampling rates, limited output calculation frequency and error arising from numerical approximations to integrals and derivatives.

Concerning prototype application, issues may include inaccuracies in data acquisition, particularly the low analogue-to-digital converter (ADC) resolution offered by commercially available microcontrollers, coupled with their limited ability to maintain constant sampling frequency. Smaller sources of inaccuracy include low data sampling rates, limited ADC responsiveness and measurement error from commercially available battery monitor integrated circuits.

2 Technology Review

Driven by current global economics and increasing environmental pressures, electric vehicles and hybrid electric vehicles (HEV) have seen an increase in popularity in recent years. Within the United Kingdom, the Society of Motor Manufacturers and Traders [5] provides data illustrating registration numbers for December 2012 and the year-to-date (full year 2012). This is shown in Table 1.

Table 1 – Electric Vehicle Registrations 2012

Vehicle Category	December			Year-to-date		
	2012	2011	% Change	2012	2011	% Change
Total pure electric	117	27	333.3	1262	1082	16.6
Plug-In Car Grant eligible	194	29	569.0	2237	1056	111.8
Total petrol/electric hybrid	1,380	1,773	-22.2	24,086	23,366	3.2
Total diesel/electric hybrid	110	1	10900.0	1284	25	5036.0
Alternatively fuelled vehicles	5	50	-90.0	687	960	-28.4

Each of these vehicles, excluding 'alternatively fuelled vehicles', relies entirely, or in part, upon one or more electric motors for propulsion. These motors convert energy provided by a battery of electrochemical cells into mechanical work. [†] Vehicles described as 'Alternatively fuelled' may rely upon bio-fuels, alcohol based fuels, solar power etc.

2.1 Electric Vehicle Types

2.1.1 Battery Electric Vehicles

Battery electric vehicles (BEV) derive tractive force wholly from one or more electric motors, where power is provided to the motor(s) by a battery pack. These vehicles traditionally fall into the category of 'plug-in electric vehicles'. A plug-in electric vehicle is described by Sandalow [6] as any electric road vehicle that can have its battery pack recharged by an external source, such as a domestic socket. For example, BEVs may draw energy from the domestic electricity grid and use it to charge their on-board battery packs. This allows BEV owners to take advantage of off-peak electricity prices and the economies of scale offered by large power generation plants. If the battery pack is charged by electricity generated from a renewable source, then these vehicles may also provide zero-emissions transport.

2.1.2 Hybrid Electric Vehicles

For tractive force, HEVs use one or more electric motors in conjunction with an ICE. As with a BEV, energy is provided to the electric motor(s) by a battery pack. Chan [7] describes an HEV as any that is propelled by both an electric motor/generator and an ICE. The motor and ICE may be

[†] *Capacitors/super-capacitors will not be considered within this report.*

arranged in either series or parallel, where the ICE offers range and the electric motor improves efficiency via energy recovery and storage. Energy recovery occurs during braking and coasting. For parallel configurations, the ICE may also provide additional tractive force when required. Hybrid electric vehicles are particularly attractive as the presence of an ICE permits the use of existing infrastructure such as filling stations, which are substantially more common than public electric vehicle charging points. The hybrid system may also reduce or eliminate the possibility of ever having to temporarily withdraw the vehicle from use purely to charge on-board batteries. Some current HEVs also feature 'plug-in hybrid' technology. Termed 'plug-in hybrid electric vehicles' (PHEV), they can be connected to an external power source to replenish the on-board battery pack when the vehicle is not in use, just as with a BEV.

2.1.2.1 Hybrid Powertrain Architecture

As Chan [7] suggests, HEVs can be categorised by powertrain architecture. There are three major formats for current HEV powertrains:

1. Series HEV, where tractive effort is provided entirely by the electric motor(s). The ICE acts as a range extending generator that can either charge the vehicle's on-board batteries or power its electric motor(s) directly. Series hybrids may be referred to as 'extended range electric vehicles' (E-REVs).
2. Parallel HEV, where tractive effort may be provided by the vehicle's ICE and its electric motor(s). Both are coupled to the driven wheels via a transmission system, and torque may be provided by ICE alone, electric motor(s) alone, or both simultaneously. Chan [7] states that there are six different modes of operation for a parallel hybrid:

   " i) Motor alone mode: engine is off, vehicle is powered by the motor only;
   ii) Engine alone mode: vehicle is propelled by the engine only;
   iii) Combined mode: both ICE and motor provides power to the drive the vehicle;
   iv) Power split mode: ICE power is split to drive the vehicle and charge the battery (motor becomes generator);
   v) Stationary charging mode;
   vi) Regenerative braking mode (include hybrid braking mode). "
3. Series-Parallel HEV, where this architecture offers both series and parallel operation. As with a parallel hybrid, tractive force may be provided by either the vehicle's ICE or its electric motor(s). However, series-parallel vehicles make it possible to decouple the ICE from the driven wheels in order to power a separate generator, permitting series operation.

2.1.3 Summary

Table 2 summarises the current architectures of electric vehicles.

Table 2 – Current EV Powertrain Architecture

Vehicle Designation	Plug-in capability	ICE present	ICE capable of providing tractive effort	ICE capable of acting purely as a generator with vehicle in motion
BEV	✓	×	×	×
Series HEV/EREV	×	✓	×	✓
Plug-in series HEV/EREV – PHEV	✓	✓	×	✓
Parallel HEV	×	✓	✓	×
Plug-in parallel HEV – PHEV	✓	✓	✓	×
Series-parallel HEV	×	✓	✓	✓
Plug-in series-parallel HEV –PHEV	✓	✓	✓	✓

Figure 1 illustrates these architectures.

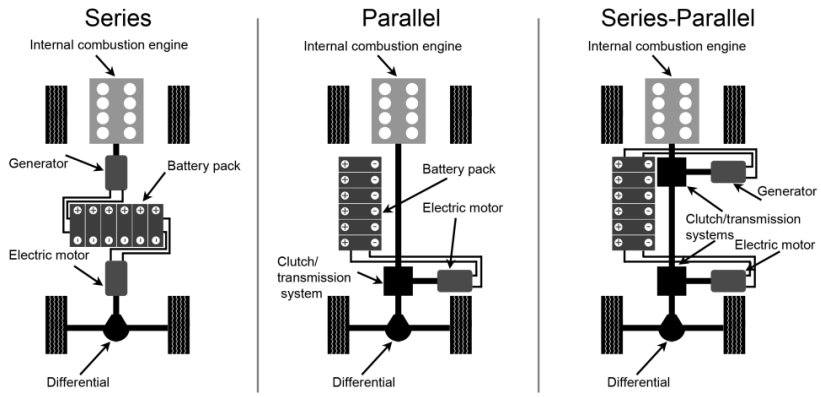

Figure 1 – Current EV Powertrain Architecture

2.2 General Battery Structure

Husain [8] describes a battery as a group of individual cells each capable of converting chemical energy into electrical energy. These cells are connected in series within each battery module casing. These battery modules may then be arranged together in both series and parallel to create a battery pack capable of producing the desired voltage, capacity and current handling capability. Each cell contains a positive and a negative electrode surrounded by an electrolyte (a substance containing ions that can be decomposed by application of direct current). The electrodes are separated by a permeable membrane known as a 'separator', which permits the flow of charged ions whilst preventing flow of electrons. Figure 2 illustrates basic cell structure, based upon information drawn from Rahn and Wang's *Battery Systems Engineering* [9].

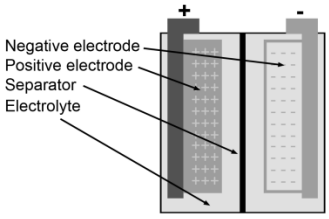

Figure 2 – Battery Cell Structure

When the cell is discharging, positive ions move from anode (negative electrode) to cathode (positive electrode), with negative ions moving in the opposite direction. Electrons flow through the connected load from anode (-ve) to cathode (+ve). During charging, the negative electrode becomes the cathode and the positive electrode becomes the anode, with electrons from an external source flowing into the cathode. The movement of charged ions is now reversed. Both charging and discharging of a simple cell are shown in Figure 3 [9].

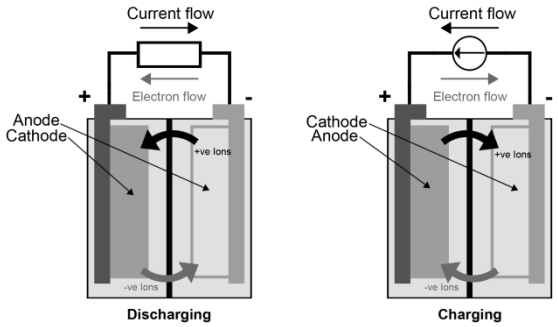

Figure 3 – Battery Cell Discharge/Charge

2.3 Primary EV Battery Types

There are three major battery types currently in use within EVs:

1. Lead-acid (Pb-acid).
2. Nickel-metal hydride (Ni-MH).
3. Lithium-ion/lithium-polymer (Li-ion/Li-poly).

Pistoia [10] describes the evolution of EV battery technology over the past twenty years. In summary, he says that the early 1990s were dominated by lead-acid technology, whilst this period also saw research into sodium-sulphur and zinc-bromine chemistries. During the middle of the decade, nickel-metal hydride chemistries became more widely available, with their improved energy density making them an attractive alternative to lead-acid. Nickel-metal hydride batteries would subsequently be used in many electric vehicles, including the Toyota Prius. During this same period, lithium-ion technology began to emerge, though concerns were raised about fire risk related safety issues. Approaching the present day, nickel-metal hydride is still dominant within the HEV sector. However, the next generation of BEVs demand the newer lithium based technology due to its much improved performance.

2.3.1 Lead-Acid

Citing Linden and Reddy's *Handbook of Batteries*, Rahn and Wang [9] state that lead-acid is a relatively old technology that holds 40-45% of the battery market. Lead-acid batteries are used frequently for starting, lighting and ignition in cars and commercial vehicles. They have also been used extensively to power electric vehicles. Larminie and Lowry [11] state that "the best known and most widely used battery for electric vehicles is the lead-acid battery."

Larminie and Lowry [11] also describe the favourable properties of lead-acid, highlighting that lead-acid batteries are cheap to produce, reliable and widely available. They offer relatively high cell voltage and have very low internal resistance. Their low cost is a product of the ease of availability and low value of the materials required to make them; i.e. lead, plastic and sulphuric acid. Their low internal resistance is an attractive property as it allows terminal voltage to be better maintained under load; lead-acid technology does not suffer a substantial drop in terminal voltage when current is drawn.

However, compared with nickel-metal hydride and lithium-ion or lithium-polymer, lead-acid batteries offer low specific energy, making them unsuitable for long range electric vehicles. Lead-acid batteries are also subject to potentially irreversible degradation, known as sulphation, if left in a state of discharge for a suitably long period. Furthermore, the process required to charge lead-acid batteries is complex. For example, Larminie and Lowry [11] describe a commonly used technique known as “multiple step charging”. During multiple step charging, charging current is applied to the battery until cell voltage reaches a desired point. Charging current is then removed and voltage allowed to drop to a second specified point, before charging current is reapplied. This process is repeated reiteratively until the battery is charged.

Rahn and Wang [9] describe the possibility of battery degradation/failure occurring as a result of corrosion and overcharging related gas generation. Other aging mechanisms include “active-material degradation” [9], where mechanical stress caused by other modes of degradation begins to damage the positive electrode, reducing the amount of active material available.

2.3.2 Nickel-Metal Hydride

Found within existing HEVs such as the Toyota Prius and Honda Insight, nickel-metal hydride chemistry offers improved specific performance when compared with traditional lead-acid. In their 1994 paper, Reisner and Klein [12] described the excellent ‘near-term’ prospects of nickel-metal hydride technology, reporting high power density (power produced per unit mass or per unit volume) and both high volumetric and gravimetric energy densities, with good performance at low temperatures. High tolerance for overcharging and reversal are also listed, with these issues cited as key for high voltage operation.

However, Rahn and Wang [9] point out that nickel-metal hydride batteries self-discharge quickly without any applied load, whilst Larminie and Lowry [11] describe the need for battery cooling with any substantial nickel-metal hydride systems, owing to the heat generated by both battery internal resistance and the exothermic reaction occurring at the negative electrode.

Rahn and Wang [9] give three major modes for nickel-metal hydride degradation:

1. Internal hydrolysis (decomposition by application of direct current) consuming water, drying cells and ultimately increasing electrolyte concentration and internal resistance.
2. Corrosion reducing material at the negative electrode, eventually causing build-up of hydrogen gas, increasing cell pressure and potentially triggering venting and water loss.
3. Deterioration of electrode materials caused by insertion and de-insertion of hydrogen atoms. This effect is increased when greater depths of discharge are reached.

2.3.3 Lithium-Ion/Lithium-Polymer

Chen et al. [13] describe lithium-ion technology as the most promising of all available battery types for electric vehicle usage. It offers superior energy efficiency and power density when compared with lead-acid and nickel-metal hydride, yielding much improved specific performance, allowing reduction in weight and volume for a given capacity. Rahn and Wang describe other favourable properties of lithium-ion chemistry, such as long cycle life and a low self-discharge rate. However, they also raise the issue of the current high initial cost involved in producing a lithium-ion system.

Citing Smith et al., Hoke et al. [14] list three possible causes of lithium-ion degradation. These are elevated battery temperature, prolonged high state of charge (SOC) and number and nature of charge-discharge cycles. Rahn and Wang [9] also provide more detailed descriptions of lithium-ion aging mechanisms. For example, it is stated that elevated temperature based aging is the product of the temperature dependent growth of a 'solid-electrolyte interface' layer on the negative electrode. This effect increases internal resistance and may be compounded if the solid-electrolyte interface layer detaches from the electrode, increasing internal resistance yet further. Loss of mobile lithium is given as another aging mechanism, where this may be the result of either corrosion or plating of the negative electrode. Plating occurs during operation at low temperatures, high charge rates and low voltages,

Lithium-polymer cells differ from lithium-ion cells in that they use a solid polymer electrolyte. Venkatasetty and Jeong [15] describe the composition of a lithium-polymer battery, which is much like that of lithium-ion, only a solid polymer electrolyte replaces the liquid/gel electrolyte of lithium-ion. This allows the solid electrolyte to be sandwiched by thin electrodes. Cells are then sealed in laminated foil to form individual units which may be grouped together to form a battery pack. As a result, the cells are thin, flexible, pressure resistant and capable of being manufactured in many different shapes.

2.4 Comparison with Alternative Methods of Energy Storage

Considering current battery technology, Rahn and Wang [9] state that batteries are efficient, safe, offer a high energy-to-weight ratio and are also often recyclable. However, concerns over cost and battery life are given as possible factors preventing more widespread adoption of battery technology. Furthermore, battery behaviour is not uniform amongst the types available to the market. Beyond cost, battery life and battery degradation, specific output limits the ability of contemporary battery powered electric vehicles to rival traditional ICE and hybrid vehicles. For example, when compared with hydrocarbon based fuels such as gasoline, it is apparent that batteries offer much lower specific energy, as shown by Husain [8]. Table 3 gives nominal energy densities for various fuels and battery chemistries [8].

Table 3 – Nominal Energy Densities of Selected Energy Storage Mediums/Sources

Energy Source	Nominal Specific Energy (Wh/kg)
Gasoline	12,500
Natural Gas	9,350
Methanol	6,050
Hydrogen	33,000
Coal (bituminous)	8,200
Lead-acid battery	*35*
Lithium-polymer battery	*200*

Considering both specific energy and specific power, Rahn and Wang [9] provide a Ragone chart (a plot of specific energy against specific power used for comparing performance of energy storage methods) comparing all three battery chemistries' performance with that of a traditional ICE. This is shown Figure 4 [9].

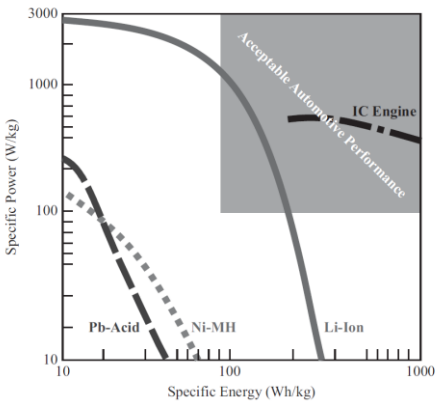

Figure 4 – Batteries & ICEs - Specific Power vs. Specific Energy

Figure 4 shows that lithium-ion chemistry does offer 'acceptable automotive performance'. However, Figure 4 also shows that the ICE system is able to achieve both high specific power and high specific energy, offering much greater specific power where energy capacity (i.e. range) is a requirement. As a result, it is clear that any electric vehicle's battery system must be optimised and well managed if it is to compete with ICE vehicles.

2.5 Comparison of Primary EV Battery Types

Rahn and Wang [9] provide data comparing lead-acid, nickel-metal hydride and lithium-ion chemistries. This is detailed in Table 4, which shows that lithium-ion is the most attractive technology for electric vehicle application.

Table 4 – Comparison of Pb-acid, Ni-MH, and Li-ion performance

	Pb-acid	Ni-MH	Li-ion
Theoretical			
Voltage (V)	1.93	1.35	4.1
Specific energy (Wh/kg)	166	240	410
Practical			
Specific energy (Wh/kg)	35	75	150
Volumetric energy density (Wh/L)	70	240	400
Energy efficiency	0.65-0.70	0.55-0.65	≈0.80
Specific power @ 80% DOD (W/kg)	220	150	350
Volumetric power density (W/L)	450	>300	>800

2.6 Battery Management

Given the characteristics of even the best performing battery chemistries currently available, it is clear that a comprehensive and well executed battery management strategy is required to ensure maximum battery performance is achieved and maintained. In the case of lithium-ion batteries, as Hoke et al. [14] state that degradation occurs mainly as a result of "temperature profile, daily charge cycling and state of charge profile", an on-board system that is capable of effectively monitoring and controlling these factors is required.

2.6.1 Key Battery Parameters

Key parameters for effective battery management are described in this section.

2.6.1.1 State of Charge, Depth of Discharge

Analogous to the fuel gauge on an ICE vehicle, Pop et al. [16] define state of charge as the percentage of maximum possible charge currently present inside a rechargeable battery. There are several available methods for estimating SOC but fundamental to all is Eq. 1, as documented by Rahn and Wang [9].

$$SOC = \frac{C_r(t)}{C} = 1 - \frac{1}{C}\int_0^t I(t)dt \qquad \text{Eq. 1}$$

where SOC is assumed to be 100% at $t = 0$ and,

C = The maximum number of ampere-hours that the battery can provide; i.e. its releasable capacity.

$C_r(t)$ = The number of ampere-hours that the battery can provide from time t.

$I(t)$ = The measured charging/discharging current, where $I > 0$ indicates discharge.

2.6.1.1.1 Voltage Lookup

Rahn and Wang [9] state that the simplest method for producing a SOC value is to utilise a one dimensional interpolation. This operation exploits a known relationship between open circuit voltage (OCV) and SOC, where OCV is the difference in electrical potential between a cell's terminals when no load is applied. In the case of lead-acid, Piller et al. [17] state that OCV has a linear relationship with SOC, though this does not apply to other chemistries. Pop et al. [16] highlight that batteries require a long rest period with no current being drawn for the result to be accurate. Coupled with the no load requirement, this required rest period ultimately renders this method unsuitable for live monitoring of an in-use pack. However, aware that these rest periods are likely to occur infrequently, Piller et al. [17] suggest that OCV based SOC estimation may be used to adjust other techniques such as coulomb counting.

2.6.1.1.2 Coulomb Counting

Eq. 1 forms the basis of the 'coulomb counting' method of estimating SOC described in Eq. 2, again sourced from Rahn and Wang [9].

$$SOC_{CC} = SOC_{CC}(0) - \frac{1}{C}\int_0^t I(t)dt \qquad \text{Eq. 2}$$

where,

$SOC_{CC}(0)$ = SOC at t = 0.

As Eq. 2 shows, this method is limited by its requirement of$SOC_{CC}(0)$. It also fails to compensate for drift arising from noise in the logged current signal [9]. One step that may be taken to improve coulomb counting accuracy is to account for operating efficiency. This approach utilises the 'depth of discharge' (DOD) metric, where DOD is the additive inverse of SOC; i.e. 0% SOC is equivalent to 100% DOD. This is given by Eq. 3.

$$DOD = 100\% - SOC \qquad \text{Eq. 3}$$

Ng et al. [18] provide a method for calculating change in DOD directly from logged battery current within an operating period τ. This is described in Eq. 4;

$$\Delta DOD = \frac{-\int_{t_0}^{t_0+\tau} I(t)dt}{C} \qquad \text{Eq. 4}$$

Charge and discharge efficiencies may then be taken into account. In each case, the efficiency is the ratio of charge in to charge out of the battery.

Calculation of charging efficiency, η_{Charge}, requires that the battery is first charged to a designated capacity at a specified rate. Rate is usually given as a fraction of a battery's listed capacity, e.g. a 10 ampere-hour (Ah) rated battery charged at '0.5C' will be charged at constant current of 5A.

Discharging then takes place at a fixed rate until the battery reaches cut-off voltage. For the purposes of their research, Ng et al. [18] specified charging at a rate of 0.6C and discharging at a rate of 0.1C, yielding an equation that can produce values for charging efficiency. This is given in Eq. 5.

$$\eta_{Charge} = \frac{C_{Discharge\ @\ 0.1C}}{C_{Charge\ @\ 0.6C}} \quad \text{Eq. 5}$$

Calculation of discharging efficiency, $\eta_{Discharge}$, requires the capacity of a given battery to be released in two stages (periods $T1$ and $T2$) [18]. First the battery is discharged to a specified DOD by constant current (I_1), then to cut-off voltage by constant current (I_2). This is described by Eq. 8;

$$\eta_{Discharge} = \frac{I_1 T_1 + I_2 T_2}{C} \quad \text{Eq. 6}$$

Efficiency compensated DOD may now be calculated [18]. This is given by Eq. 7.

$$DOD(t) = DOD(t_0) + \eta_{Discharge} \Delta DOD \quad \text{Eq. 7}$$

Therefore an improved value for SOC can be calculated by considering operating efficiencies.

2.6.1.1.3 Other Methods for SOC Estimation

Other methods for estimating SOC are described by Pop et al. [16] and Piller et al. [17]. A number of these methods are summarised in Table 5, alongside OCV and coulomb counting based approaches.

Table 5 – SOC Estimation Methods

Technique	Applications	Advantages	Disadvantages
Open circuit voltage	Pb-acid, Li-ion/Li-polymer, zinc-bromine	Easy, cheap	Long rest period required
Coulomb counting	All battery types	Accurate if frequently re-calibrated and current measurement is precise	Sensitive to parasitic reactions, costly for accurate current measurement, must be re-calibrated often, requires initial SOC to be known
Discharge test	All battery systems – used to determine initial battery capacity	Easy, accurate	Offline, time consuming, may affect battery performance permanently
Electrolyte test	Pb-acid (refractometry/specific gravity)	Possible online, helpful in determining state-of-health (see 2.6.1.2)	Sensors may be unstable in acidic electrolyte, sensitive to temperature and impurities, some batteries are sealed preventing access to electrolyte
Impedance spectroscopy	All battery types	Helpful in determining state-of-health (2.6.1.2)	Expensive, temperature sensitive
Artificial neural network	All battery types	Online	Requires 'training' data from similar battery, expensive
Kalman filter	All battery types	Online	Difficult to implement accounting for the required number of parameters

2.6.1.2 State of Health

Importantly, neither the coulomb counting nor voltage look-up methods detailed in 2.6.1.1 consider battery hysteresis effects. Some consideration of the battery's past use and resulting

performance deterioration could therefore improve SOC calculation and be used to give an indication of overall battery health.

State of health (SOH) indicates a battery's point in its life cycle and is defined by Pop et al. [16] as "a 'measure' that reflects the general condition of a battery and its ability to deliver the specified performance in comparison with a fresh battery." SOH is sensitive to factors including number of completed charge and discharge cycles, operating SOC, discharge rates and battery temperature. Pop et al. [16] also state that SOH is likely to be unpredictable and that, accordingly, an adaptive strategy such as those based upon neural networks, Kalman filtering or fuzzy logic may be required. However, Ng et al. [18] provide a more easily calculated metric for SOH estimation. This is shown in Eq. 8.

$$SOH = \frac{C_{Achievable}}{C_{Rated}} \qquad \text{Eq. 8}$$

2.6.2 Cell Balancing

According to Wen [19], imbalance is a problem common to all batteries composed of series connected cells. Arising from differences between individual cells (internal resistance, capacity, self-discharge rate etc.), the SOCs of the various cells within a battery pack may drift apart over time. Daowd et al. [20] also discuss the effect of temperature on balance, stating that non-uniform temperature distribution across the battery pack will create uneven cell self-discharge rates. Variation in cell SOCs may lead to permanent cell damage, impacting SOH and achievable SOC. For many chemistries, cells may suffer degradation as a result of particularly low SOC. Equally, when charging, cells with greater SOC may be overcharged, another possible cause of battery ageing. To try and combat cell damage, prolong battery life and maximise battery performance, many BMS systems feature cell balancing capability. This system may be either passive or active.

Daowd et al. [20] describe a passive system as one that removes charge from the more charged cells through a passive resistor until SOC equilibrium is achieved. This method wastes charge, converting electrical energy into heat. Based on the work of Cao et al. [21], Figure 5 provides an example of simple dissipative system, where the BMS is capable of controlling resistor switching;

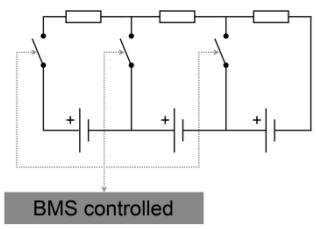

Figure 5 – Dissipative Balancing System

Conversely, the balancing system may be active, opting to move charge from cells with greater SOC into those with lower SOC. Active systems offer greater efficiency due to reduced energy wastage, though a more complex control strategy may be required. Daowd et al. [22] describe several active balancing techniques, which are summarised alongside passive balancing in Table 6.

Table 6 – Cell Balancing Methods

Method	Type	Summary
Shunting resistor	(Passive)	Energy drawn from cells with greater SOCs is converted into heat, equalising cell pack charge levels. This method requires a control system to assess individual cell SOCs and operate switching/balancing accordingly, discharging cells with high SOCs.
Switched capacitor (SC)	Capacitive shuttling (Active)	A number of switched capacitors (n-1 capacitors in a pack with n cells), each connected in parallel 'between' two cells, allow current to be drawn from cells with high SOCs, charging the relevant capacitor. This capacitor can then discharge into the next series connected cell. This switching and charging/discharging is repeated at constant frequency, eventually yielding cell balance.
Single switched capacitor (SSC)	Capacitive shuttling (Active)	As with the SC system, however only one capacitor is used. A number of switches (n+5 for n cells) appropriately configured allow any given cell to charge the capacitor before it is discharged into the desired second cell. This method requires a control system to assess individual cell SOCs and operate switching/balancing accordingly, charging the capacitor whilst connected to cells with high SOCs and discharging into those with low SOCs.
Double-tiered switched capacitor (DTSC)	Capacitive shuttling (Active)	As with the SC system, however a second 'tier' of capacitors are added in parallel to the first, reducing balancing time.
Modularised switched capacitor (MSC)	Capacitive shuttling (Active)	As with the SC system, however the given number of cells constituting the battery are separated into individual 'modules' – each containing their own SC cell balancing system. A second SC equalisation system between modules may be used, reducing switch voltage and current stress [22].
Switched inductor (SI)	Inductor /transformer balancing (Active)	Switched inductor systems may be single inductor (SSI) or multiple inductor (MSI), each of which operate analogously to the SSC and SC systems described above. However, they utilise inductors rather than capacitors as the means of temporary energy storage.
Single-winding transformer (SWT)	Inductor /transformer balancing (Active)	SWT systems operate in a similar way to SSC/SSI systems described above. However, rather than employing separate temporary energy storage that may be charged and discharged, they use 'pack-to-cell' or 'cell-to-pack' methods [22]. During 'pack-to-cell' operation, switches are configured so that full pack output is connected to a weak (low SOC) cell via the transformer, charging that particular cell whilst discharging the rest of the pack. During 'cell-to-pack' operation, a strong (high SOC) cell is connected to the full pack via the transformer, reducing that cell's SOC whilst charging the rest of the pack.
Multi-windings transformer (MWT)	Inductor /transformer balancing (Active)	Multi-windings configurations may be described as utilising a 'shared transformer' [22]. The system has one magnetic core, with one winding connected around each cell and a further winding connected around the full pack. These systems may take either 'forward' or 'flyback' structure. In forward systems, the cell with the highest SOC is discharged via the transformer, charging the full pack. In flyback systems, the full pack is connected to the transformer, with the transformer storing some energy. When this connection is broken, the stored energy is released and used to charge the weakest cells.
DC-DC converter	Energy converter balancing (Active)	Numerous DC-DC converter systems such as the Ćuk, Buck-boost and flyback converters may be used. As with other methods, these use pack power to charge weak cells, or use strong cell power to charge the pack. These systems tend to require complex control systems and are expensive to implement [22].

Single switched capacitor systems offer the lowest cost of all the active balancing methods available. Figure 6 shows a single switched capacitor system like that described by Daowd et al. [22].

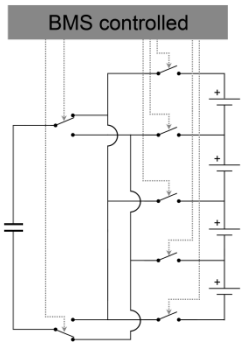

Figure 6 – Single Switched Capacitor Balancing System

2.6.3 Hardware & Software

The BMS system consists of both hardware and software. The software protocol is an instruction set that controls the various hardware elements of the BMS system, whilst also performing the calculations required to track key performance metrics. This protocol is ultimately compiled and embedded on a control unit which is capable of receiving sampled battery pack data via one or more cell monitor and data acquisition (DAQ) circuits. Figure 7 illustrates example BMS hardware;

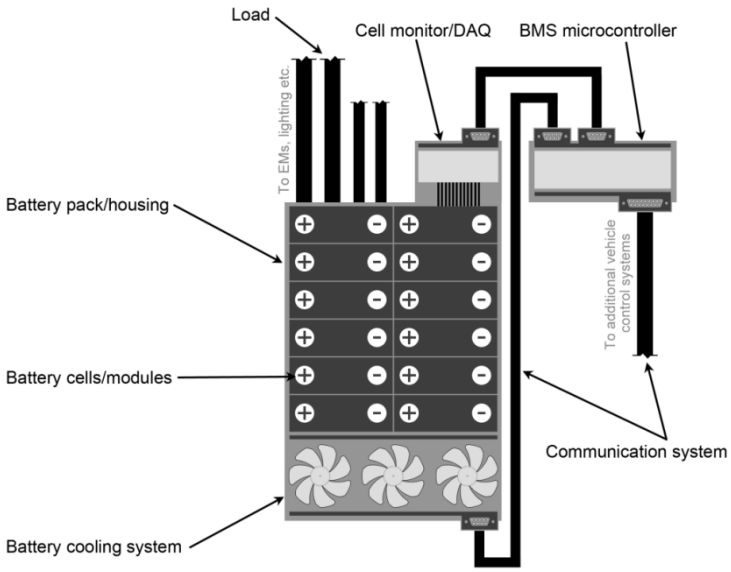

Figure 7 – BMS Hardware

Considering software, the BMS protocol is capable of assessing various battery parameters and responding where necessary by balancing cells, increasing cooling or activating vehicle error modes. Data is logged to the controller's memory, where each logged parameter is received at a given sample frequency and then processed further if required. Parameter processing takes place at a specified frequency, though this frequency may vary between blocks of parameters.

2.7 Dynamometer Drive Cycles

Forming an important part of vehicle testing, a dynamometer drive cycle is a data set describing vehicle speed against time. Created by official bodies such as the US Environmental Protection Agency (EPA) and the United Nations Economic Commission for Europe (UNECE) World Forum for Harmonization of Vehicle Regulations, these data sets are used as inputs for chassis dynamometers so that vehicle parameters such as emissions and fuel consumption can be measured under standard operating conditions. Sometimes referred to as drive schedules, they also form useful inputs for vehicle simulation, permitting a vehicle's behaviour to be modelled based on its speed at any point in the cycle. There are four major drive cycles contained considered within this research. These are:

1. New European Drive Cycle (NEDC).
2. EPA FTP-75.
3. EPA UDDS.
4. EPA US06.

All EPA schedules have been sourced from their website [23], whilst the NEDC data has been recovered from a figure in Barlow et al.'s '*A reference book of driving cycles for use in the measurement of road vehicle emissions'* [24].

The four considered schedules are shown in Figure 8.

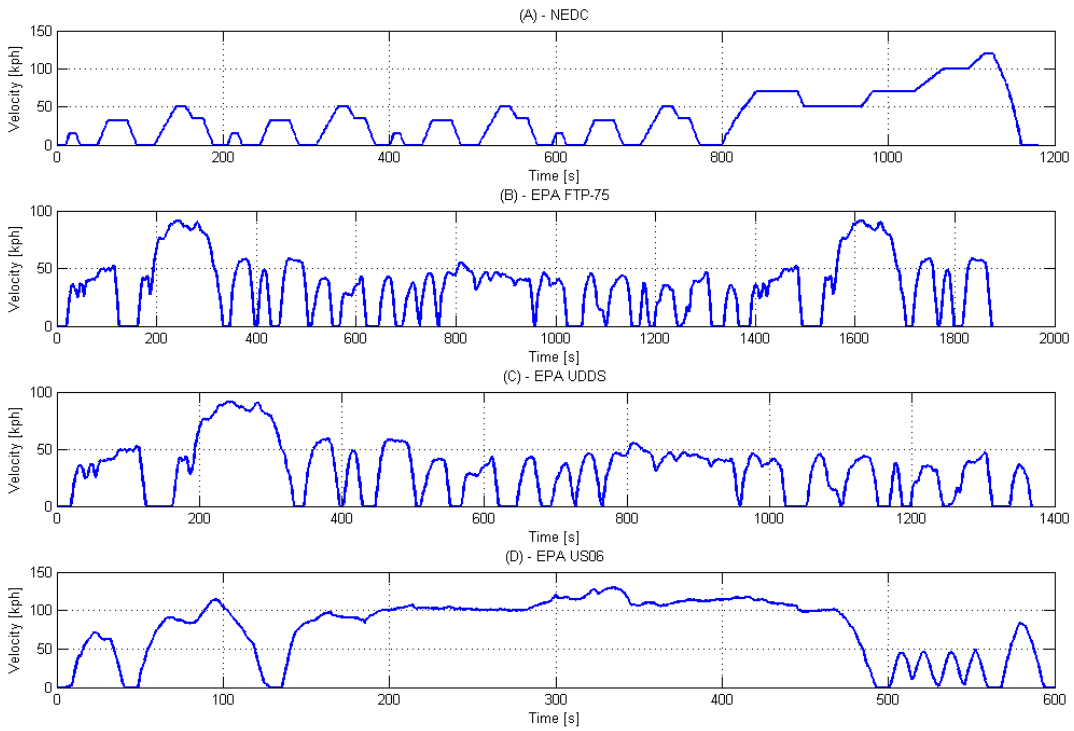

Figure 8 – Considered Drive Cycles

3 Methodology

3.1 Initial Protocol Structure

The initial stages of protocol development involved establishing each of the required BMS operations and the order in which they must be performed. Giving priority to safety related parameters and fault diagnostics, the protocol structure first iterates through a number of safety checks. If these checks are passed, then battery SOC and SOH are calculated. If they are failed, then appropriate action is taken, whereby the vehicle is either shutdown or 'limp mode' is enabled to prevent damage or injury. This structure is shown in Figure 9.

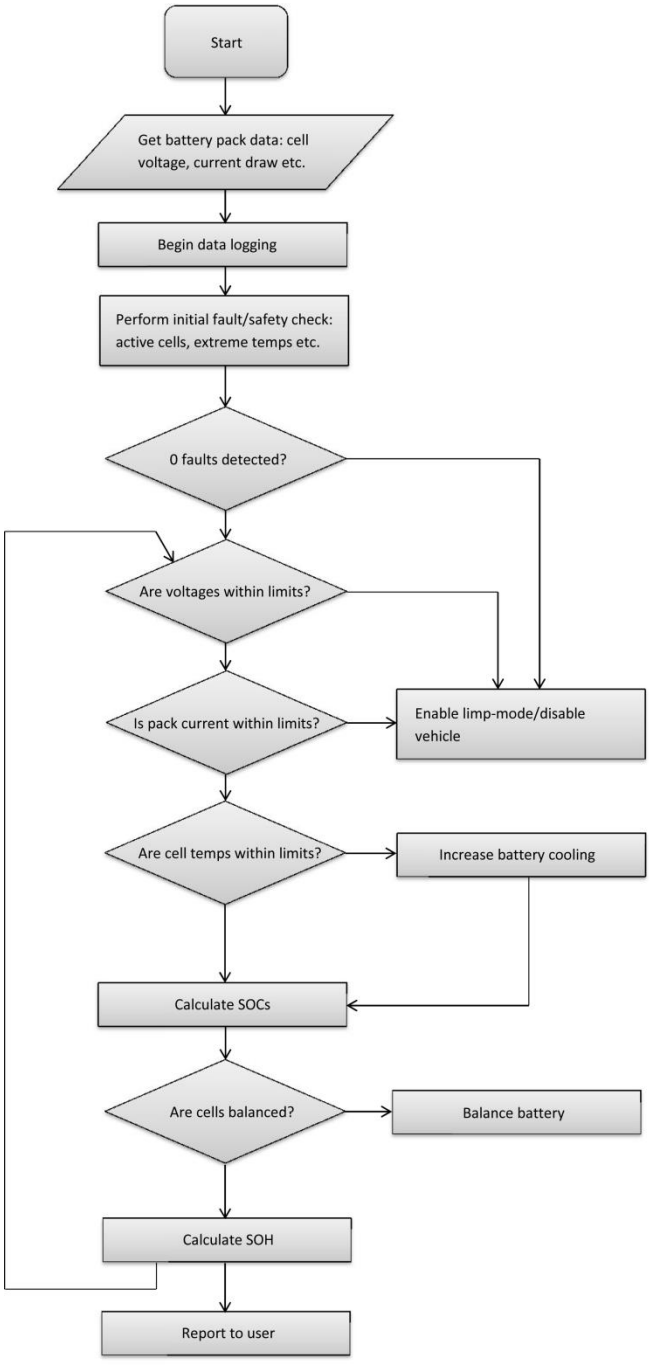

Figure 9 – BMS Protocol Structure

3.2 Software Simulation

To permit development of the basic BMS protocol that could later be ported to relevant hardware, a MATLAB based electric vehicle simulating software package was first created. This software package, dubbed 'EV Sim Tool', allowed a high-level battery management instruction set to be created and developed as required. To achieve this, the software had to be capable of accurately emulating the conditions and inputs encountered by a real-world BMS. There are four key parameters which must be monitored by an effective BMS:

1. Current draw from the battery pack.
2. Battery and cell voltages.
3. Battery temperature.
4. Battery age; both cycle number and calendar age.

From these core input parameters, a large number of useful metrics may then be calculated by the BMS software and used for additional battery management processes and user reporting. A number of screenshots are shown in Appendix B.

3.2.1 Software Structure

Without access to a real vehicle battery system, it was necessary to develop a responsive method for generating data representative of a true electric vehicle. As the BMS protocol had to be capable of both influencing and responding to this data, the developed software package operates by taking a limited number of user defined inputs and using them to create the parameters that the BMS requires to function effectively. The BMS section then performs relevant calculations with these parameters, and may subsequently feed data back into the modelling loop. Figure 10 illustrates the basic flow of data within the software package, from user inputs such as dynamometer drive cycles and vehicle kerb weight, through the required models and calculation routines, into model and user feedback.

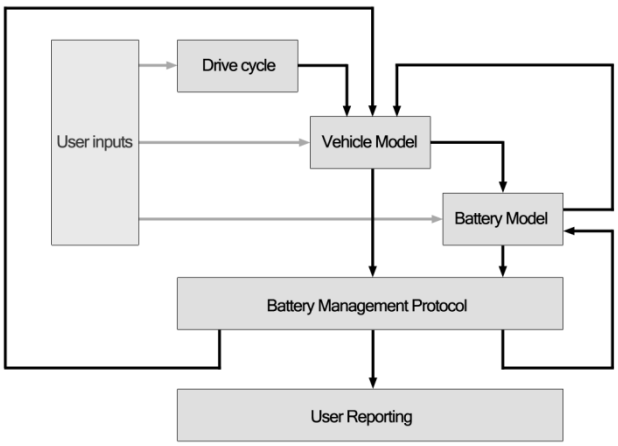

Figure 10 – EV Sim Tool Data Flow

3.3 Simulating Vehicle Behaviour

In order to generate representative datasets for an electric vehicle's electrical parameters, it is necessary to consider the process by which electrical energy from the vehicle's battery pack is converted into mechanical work at the driven wheels. In the case of the simulation software package, a fundamental calculation input is a dynamometer drive cycle. A drive cycle is composed of two elements; one vector of sample times and a second, corresponding vector of vehicle road speeds. Given this drive cycle data, in combination with a small number of supplementary input parameters, the software then calculates a power demand that the battery pack must achieve if the vehicle is to meet the drive cycle's speed request.

To calculate power demand, the software's vehicle model recursively evaluates Newton's second law at every point throughout the drive cycle, calculating the tractive force required to enable the vehicle to meet instantaneous velocity and acceleration demand, whilst also considering both aerodynamic and tyre drag forces. This is described by Eq. 9.

$$\forall\, t \in DriveCycle:\ F_{Tractive}(t) = [m_{Car} \cdot a_{Car}(t)] + F_{Drag_{Tyre}}(t) + F_{Drag_{Aero}}(t) \qquad \text{Eq. 9}$$

where,

$$a_{car}(t) = \frac{dv_{Car}(t)}{dt} \qquad \text{Eq. 10}$$

and,

F = Force
t = Sample time
m = Mass
a = Acceleration
v = Velocity

Aerodynamic drag, F_{Drag_Aero}, is modelled on the drag characteristics of a 2009 BMW E90 3 Series [25, 26], though frontal area and drag coefficient values are fully user editable. The value for instantaneous aerodynamic drag is given by Eq. 11.

$$F_{Drag_{Aero}}(t) = \frac{\rho_{Air} \cdot v_{Car}(t)^2 \cdot A_{Frontal} \cdot K_D}{2} \qquad \text{Eq. 11}$$

where,

ρ = Density
A = Area
K_D = Drag coefficient

Tyre drag, F_{Drag_Tyre}, utilises a pressure and velocity dependent model consistent with SAE J2452 [27] standard, as given by Eq. 12.

$$F_{Drag_{Tyre}}(t) = n_{Wheels} \cdot p^{\alpha} \cdot {F_N}^{\beta} \cdot [K_A + (K_B \cdot |v_{Car}(t)|) + (K_C \cdot v_{Car}(t)^2)] \qquad \text{Eq. 12}$$

where,

p	=	Tyre pressure	n_{Wheels}	=	number of wheels, i.e. 4
F_N	=	Normal force, i.e. $m \cdot g$ (assume no aerodynamic lift/downforce)	$\alpha, \beta,$ $K_A, K_B,$ K_C	=	User definable approximating coefficients, i.e. tyre model parameters. Values provided by The MathWorks are used throughout [28].

Figure 11 shows tyre and aero drag experienced by a car of mass 1400kg, with frontal area 2.54m^2 and drag coefficient 0.26, across a speed range of 0 – 140 kph.

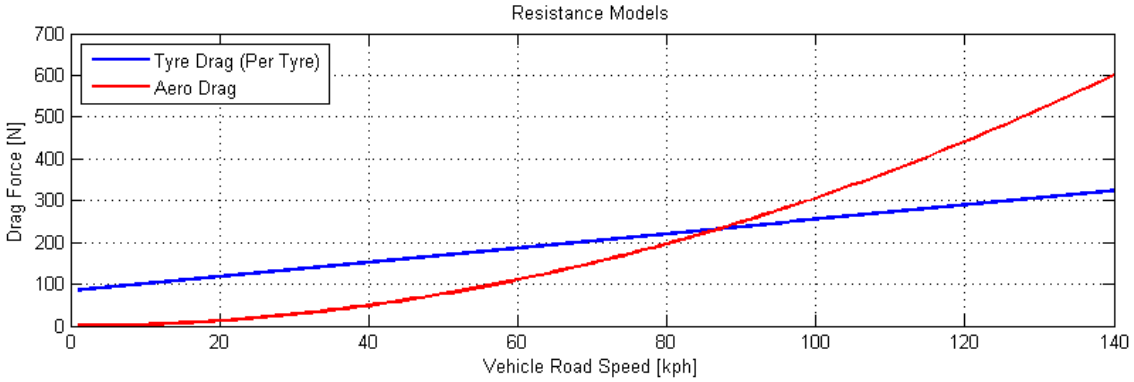

Figure 11 – Rolling & Aero Resistance

Using the results of Eq. 9 – Eq. 11, it becomes possible to calculate power at the vehicle's driven wheels, as described by Eq. 13.

$$P_{Wheel}(t) = F_{Tractive}(t) \cdot v_{Car}(t) \qquad \text{Eq. 13}$$

Then, by taking a factor of drivetrain efficiency and considering possible parasitic loads such as cooling, lighting etc., battery pack power demand may be calculated by application of Eq. 14

$$P_{BatteryPack}(t) = \frac{P_{Wheel}(t)}{\eta_{Drivetrain}} + P_{Parasitic}(t) \qquad \text{Eq. 14}$$

This power demand may then be used as a driving input to the battery model described in 3.4.

3.4 Simulating Battery Behaviour

Though more purely mathematical modelling of battery behaviour has been described by authors such as Knauff et al. [29] and Gholizadeh and Salmasi [30], these methods require some degree of validation against recorded data to ensure accuracy. For the purposes of this research, however, a less complex interpolation based strategy has been adopted. This approach permits a large degree of flexibility to be written into the simulation software, where mapped data characterising battery behaviour may be stored for any number of battery chemistries, architectures and sizes. Fundamental to this method is an accurate dataset for the relevant battery. As there is a desire to track both battery SOC and SOH, whilst also being able to accurately model the behaviour of a battery under load, there are a number of data sets that must be obtained for each battery to be considered. These must characterise three behaviours:

1. Terminal voltage response to charging/discharging current and SOC, including any associated effect on usable short-term capacity.
2. Terminal voltage response to temperature and SOC, including any associated effect on usable short-term capacity.
3. Long-term capacity response to cycle count.

The following supplementary information also offers potential for improved SOH determination:

- Long-term capacity response to charging/discharging current.
- Long-term capacity response to temperature.
- Long-term capacity response to operating SOC.

This data would permit a highly effective 'logbooking' strategy to be enacted, offering simulation of high accuracy SOH calculation. Where the data has proved unavailable, representative 'placeholder' values have been used.

The information used for description of the software based modelling process has been sourced from Panasonic [31]. Their 3.28Ah UPF476790 'pouch type' cell has similar packaging and performance characteristics to those used for electric vehicle application by vehicle manufacturers such as Nissan [32].

3.4.1 Current Dependent Cell Discharge Characteristics

The first item that is required is a discharge voltage map, which records cell terminal voltage at specified discharge rates against capacity discharged. This map can be obtained through logging a single cell's voltage response to specified constant current discharge rates, though for the purposes of this research, all data has been taken from published specifications. For example, Figure 12 shows discharge data for the Panasonic UPF476790 cell [31].

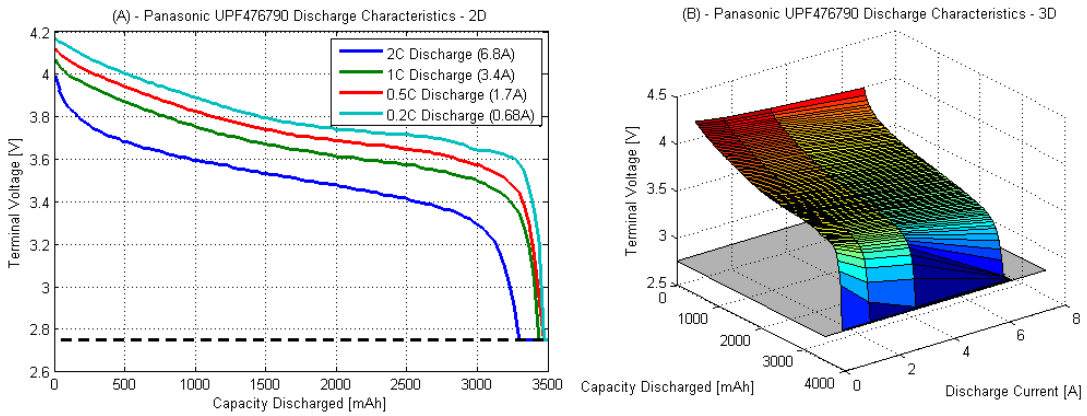

Figure 12 – Terminal Voltage Map

As Figure 12 shows, cell terminal voltage at constant temperature is a function of both load and SOC, complicating the process of modelling the voltage and current combination required to achieve a specific power output at a specific SOC.

3.4.2 Temperature Dependent Cell Discharge Characteristics

Further complicating matters is the effect of temperature on cell performance. As cell terminal voltage and capacity show greater sensitivity to temperature than to discharge rate, temperature monitoring is vital for calculation of instantaneous battery capacity and therefore also for accurate, continual SOC determination. Figure 13 illustrates this temperature sensitivity.

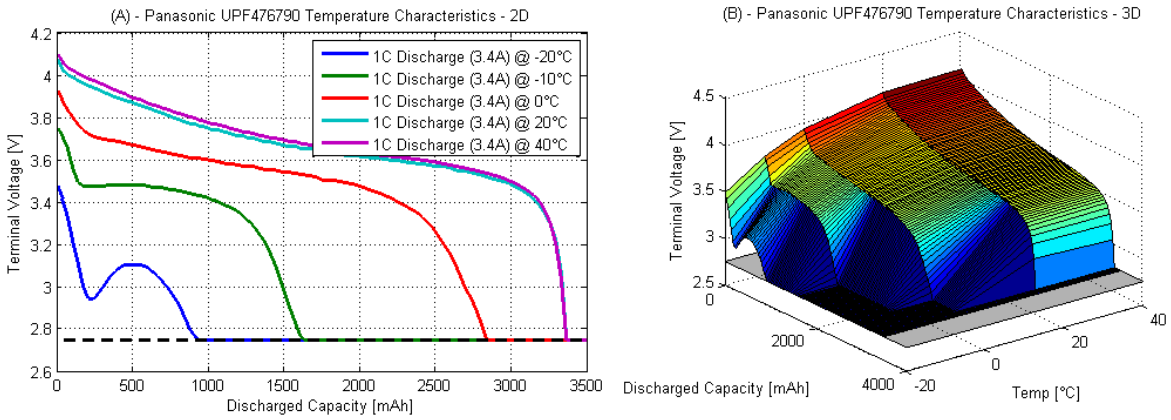

Figure 13 - Cell Temperature Sensitivity

Figure 13, in particular, highlights the vulnerability of lithium-ion chemistry to low temperatures. Ideally, operation in this region should be avoided completely. However, for completeness, it is possible to factor this data into the battery simulation/BMS protocol's calculations. Ultimately targeting a robust method for calculating cell voltage, an approach is required where SOC, current draw and cell temperature are all accounted for, as indicated by Eq. 15.

$$V_{Cell} = f(SOC, I_{Discharge}, T) \qquad \text{Eq. 15}$$

To enable this calculation via an interpolation based strategy, it is necessary to create a three dimensional data set; essentially correcting temperature dependent discharge data for discharge rate effects, then stacking the resulting 2D data grids on top of one another. This is achieved by first calculating terminal voltage ratios (relative to 1C discharge at which temperature data was logged) at each value of cell capacity discharged for each of the discharge rates shown in Figure 12. This process is described by Eq. 16.

$$\forall\, I_{Discharge} \in DischargeRates: \quad r_{Voltage\_I_{Discharge}} = \frac{V_{Terminal_{I_{Discharge}}}}{V_{Terminal_{I_{1C}}}} \qquad \text{Eq. 16}$$

Each of the data series describing response to temperature are then multiplied by the relevant ratio, yielding four curves (0.2C, 0.5C, 1C, 2C) for each temperature. This is shown in Figure 14.

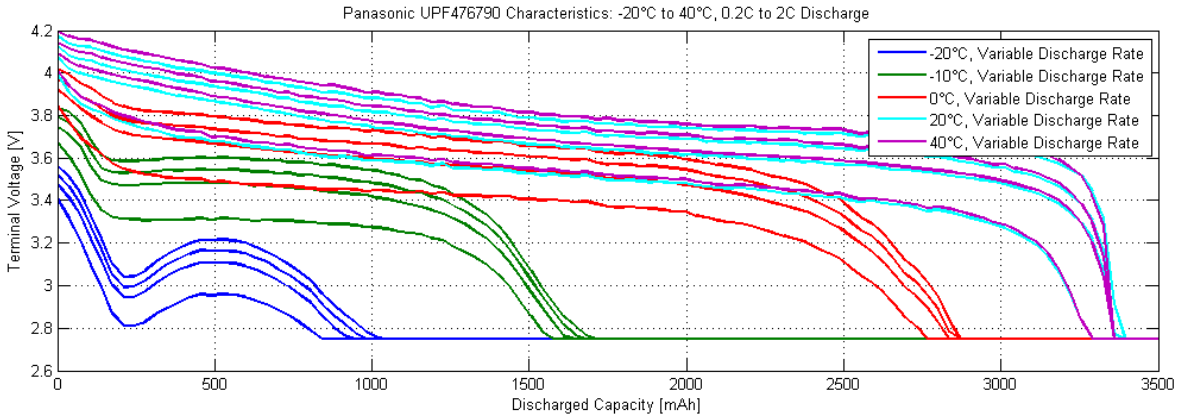

Figure 14 - Combined Discharge Rate & Temperature Characterisation

From the three dimensional data set characterising cell voltage response to temperature, discharge rate and discharged capacity, it is then possible to satisfy Eq. 15 via 3D interpolation. However, given that the inputs to the battery model will be power demand, SOC and temperature, it is more useful to create maps representing cell power. To achieve this, all terminal voltage values are multiplied by their corresponding discharge current axis values, yielding maps that give cell power as a function of temperature, discharge current and capacity discharged. This is described by Eq. 17 and illustrated in Figure 15.

$$P_{Cell} = I_{Cell\_Discharge} \cdot V_{Cell\_Terminal} \qquad \text{Eq. 17}$$

where $V_{Cell\_Terminal}$ is given by Eq. 15.

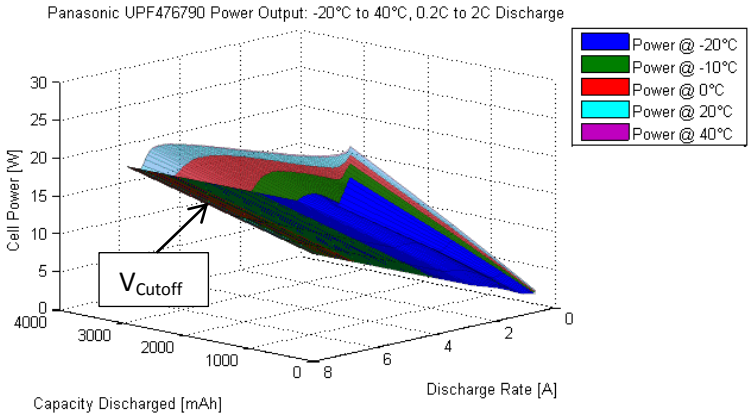

Figure 15 – Cell Power Maps

Indicated on Figure 15 is a 'V_{Cutoff} Plane'. This planar section of the plot is a result of the manufacturer specified 2.75V cell cut-off voltage, and the cell should not be operated in this region.

3.4.3 Battery Pack Power Capability

Where individual cell power characteristics are known, this information can be used in conjunction with battery pack configuration data to calculate the entire battery pack's power

capability. It is necessary to know how the battery's cells are arranged, as this determines pack voltage, capacity and peak current handling. Throughout this report, series and parallel configuration information will be referred to as 'height' and 'width'. For example, a battery consisting of six cells in total, arranged in two parallel connected banks of three series connected cells, would be said to have height 3 and width 2. Elsewhere, this configuration may be referred to as '3S2P'. This concept is illustrated in Figure 16 – Battery Cell Configuration.

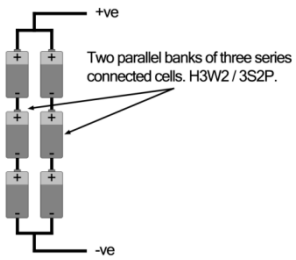

Figure 16 – Battery Cell Configuration

To calculate a full battery power map, the cell power map must be multiplied by both pack width and pack height. Importantly, increasing pack width results in increased current handling capability. Therefore the cell power map's discharge current axis must also be multiplied by pack width. This is described by Eq. 18 and Eq. 19.

$$P_{BatteryPack} = P_{Cell} \cdot Width_{Battery} \cdot Height_{Battery} \quad \text{Eq. 18}$$

$$I_{Discharge\_Axis\_Battery} = I_{Discharge\_Axis\_Cell} \cdot Width_{Battery} \quad \text{Eq. 19}$$

Figure 17 illustrates this methodology applied to a hypothetical battery composed of 4000 Panasonic UPF476790 cells (height: 80, width: 50).

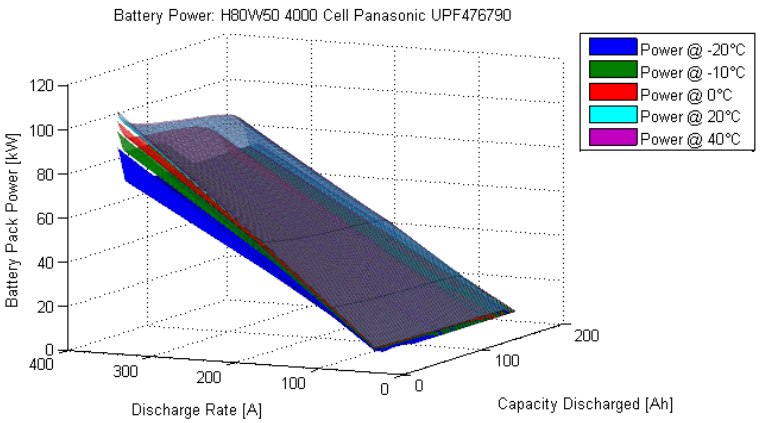

Figure 17 – Battery Power Map

3.4.4 Determining Discharge Current Required to Meet Power Demand

With battery power characterised, it is then possible to find the current and voltage combination required to achieve a given power demand at a given temperature. Eq. 20 highlights that power is a function of three inputs, as with Eq. 15.

$$P_{BatteryPack}(t) = P_{Demand}(t) = f(SOC(t), I_{Discharge}(t), T(t)) \quad \text{Eq. 20}$$

This may be arranged to form Eq. 21.

$$I_{Discharge}(t) = f(SOC_{Battery}(t), P_{Demand}(t), T(t)) \quad \text{Eq. 21}$$

Then, as power demand has already been calculated (Eq. 14), and as SOC is tracked from the battery's first cycle and is therefore always known, the necessary discharge current may be calculated provided temperature is given. This is achieved by employing a three stage 'reverse' interpolation technique, whereby three operations take place:

1. A 3D interpolation is performed to yield a temperature specific, 2D battery power map.
2. A 2D interpolation is performed to yield a 1D curve or 'section' through the 2D power map at the specified state of charge.
3. A 1D interpolation is performed on this curve to find the discharge current at which power demand is met.

Figure 18 illustrates the sectioning of a 2D map (23.83°C) at an example SOC of 65.39%, where this is the average of all pack cells. This SOC value is taken at the last calculated discharge rate and temperature; i.e. the previous drive cycle sample point.

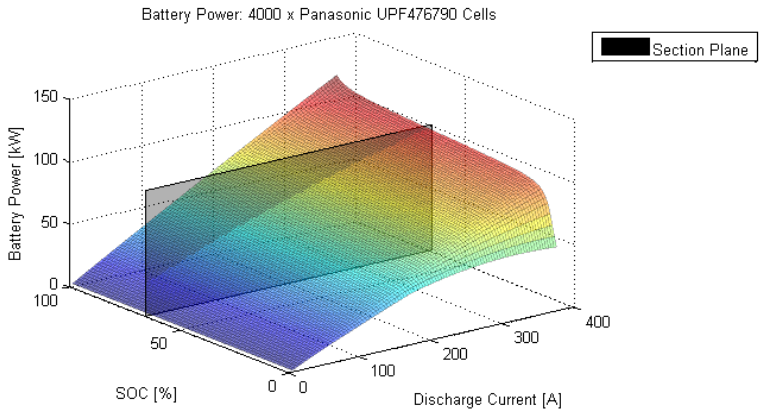

Figure 18 – Power Map Sectioning

Figure 19 shows battery power plotted on the section plane. The 20.9kW power demand issued at this point in the relevant drive cycle is also shown, where this is achieved at 68.87A discharge.

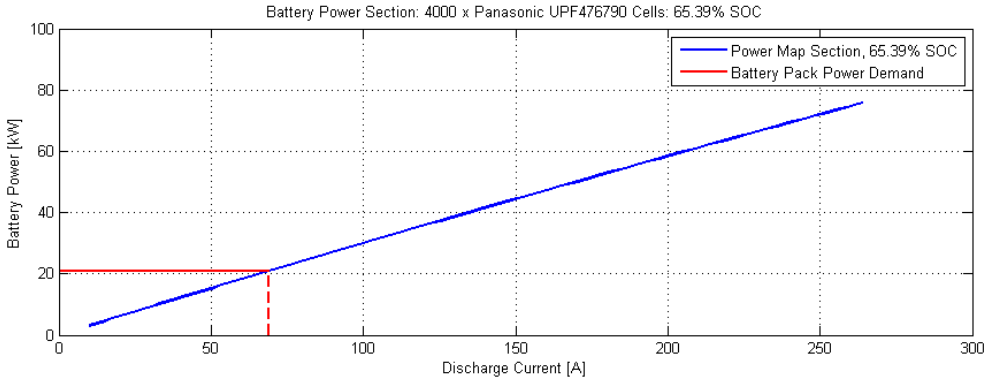

Figure 19 – Final Discharge Current Determination

To determine battery terminal voltage, power demand may be divided by discharging current, permitting accurate voltage response to applied load to be simulated. This is given by Eq. 22.

$$V_{Terminal}(t) = \frac{P_{Demand}(t)}{I_{Discharge}(t)} \quad \text{Eq. 22}$$

3.4.5 Cycle Life Behaviour

The relationship between cycle count and long term battery capacity or SOH is achieved through interpolation of a 1D curve. In the case of the Panasonic UPF746790, the manufacturer data sheet provides the cycle life information shown in Figure 20.

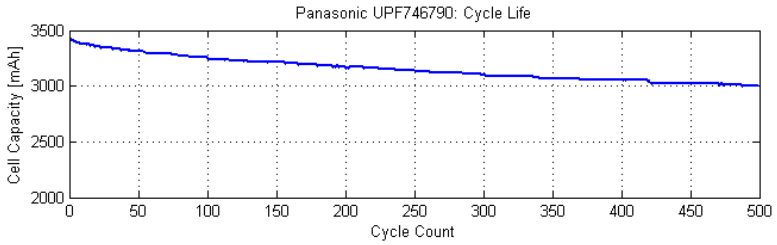

Figure 20 - Cycle Count & Capacity

This information allows a simple SOH calculation strategy to be employed, whereby,

$$SOH = \frac{C_{Current}}{C_{Initial}} \quad \text{Eq. 23}$$

where,

$$C_{Current} = f(nCycles) \quad \text{Eq. 24}$$

However, this method does not account for long term capacity loss arising from prolonged or extreme operating temperatures, discharge rates or states of charge.

3.4.6 Long Term Capacity Response

One method for improving SOH calculation is to consider battery long term to response every unit of time spent operating at a certain condition. For example, every second spent operating at -20°C may cause a small percentage loss in overall long-term capacity. The same is true for both discharge rate and SOC, as well as temperature. Accordingly the simulation software includes the functionality for lookup tables that account for this behaviour. Some example data is illustrated in Figure 21.

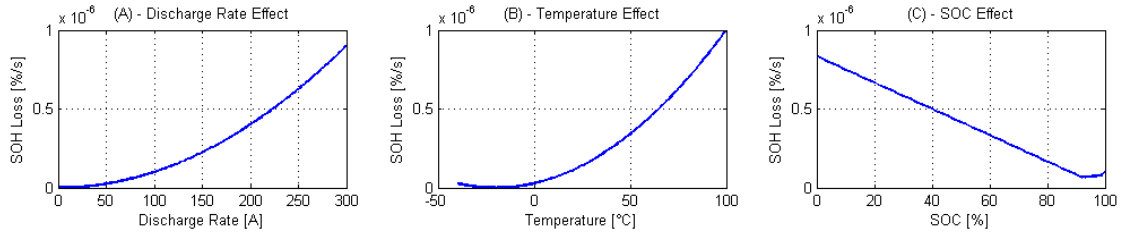

Figure 21 - Improved SOH Strategy

The simulated BMS may then assign a SOH loss for each sampled operating condition. A summation of these losses then offers total operating SOH loss, and may be used to calculate a more accurate SOH value. Considering calendar effects, a constant percentage SOH loss per year may be considered; a value of 1% per calendar year has been applied to the simulation.

3.4.7 Charging

Charging is modelled through the use of charge profiles. A charge profile may be loaded, then a charging time or charged capacity specified. After this, the charging process is simulated and the battery's logbook file updated to reflect the change in battery SOC. An example profile is given in Figure 22, sourced from Panasonic [31].

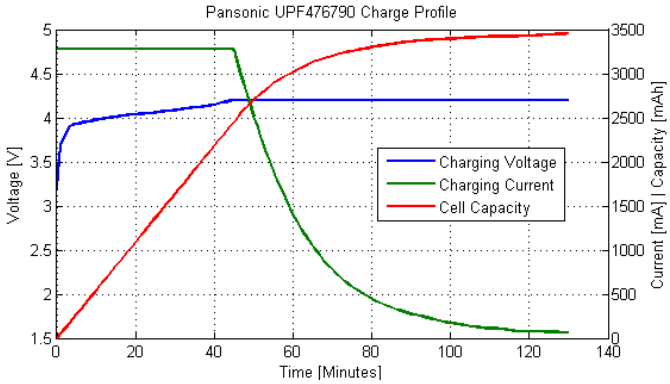

Figure 22 - Panasonic UPF476790 Charging Profile

In Figure 22, it may be seen that the applied profile uses a constant current – constant voltage charging method. However, provided there is data characterising cell charging current, charging voltage and resulting capacity, any charging method may be simulated.

3.4.8 Battery Imbalance

One feature which is not modelled is the process by which a battery becomes unbalanced. To enable adequate protocol testing, the software user may simply generate a randomised SOC profile, clipped to user specified upper and lower bounds.

3.5 Simulation Strategy

To enable effective testing of the BMS protocol, the simulation must account for a number of additional items. For example, these include:

- Simulating battery temperature.
- Simulating parasitic losses.
- Simulating cell balancing and cell balancing methods.
- Accounting for over-current or over-power limit demands that the battery pack is unable to meet.

3.5.1 Temperature & Parasitic Losses

To introduce variation in temperature inputs and test this aspect of the modelling strategy, the battery model routine simply scales and offsets power demand to give pack temperature value as described by Eq. 25.

$$T_{BatteryPack}(t) = 20 + \left(\frac{P_{Demand}(t)}{P_{MaxAchievable}}\right) \cdot 20 \quad \text{Eq. 25}$$

Parasitic losses are also calculated in the same way, as shown in Eq. 26.

$$P_{Parasitic}(t) = 1000 + \left(\frac{P_{Demand}(t)}{P_{MaxAchievable}}\right) \cdot 2000 \quad \text{Eq. 26}$$

where power is measured in W.

3.5.2 Cell Balancing

Cell balancing can be modelled in two ways; dissipative and active. Dissipative balancing simply rejects a quantity of energy from the most charged cell in the battery pack, turning it into waste heat. Active balancing is modelled as either 'cell-to-pack', or 'pack-to-cell', either shuttling energy from the most charged cell to the entire pack or from the entire pack to the least charged cell. In both cases, balancing discharge current is assumed to be low enough to have no influence on previously calculated terminal voltage. Therefore, Eq. 27 may be applied.

$$I_{Balancing} = \frac{V_{Terminal}}{R_{Balancing}} \quad \text{Eq. 27}$$

Where charge shuttling is modelled, an efficiency constant is applied to calculate rate of charge returned to the system and thus Eq. 28 may be applied.

$$I_{Balancing\_Recovered} = I_{Balancing} \cdot \eta_{Balancing} \quad \text{Eq. 28}$$

3.5.3 Limit Events

When a battery pack current or power demand is issued that the modelled battery pack is unable to meet, the simulation process is able to respond. It achieves this by first clipping maximum output power to the maximum available. It then feeds this information back to the vehicle model and triggers a recalculation. In this way, it is possible to simulate events where the vehicle is actually unable to meet the specified drive cycle due to low battery SOC, active limp-mode condition or battery failure.

3.6 BMS Protocol Development

Ultimately, the described vehicle and battery modelling techniques exist purely to permit the development and testing of a template battery management protocol. The model outputs

function as BMS inputs, mimicking the relevant sensor channels that a real world BMS system would monitor.

To facilitate efficient programming and code development, a variable naming convention was adopted, whereby a prefix denoting parameter type is followed by a natural language description of that parameter. Following this naming convention, key parameters and their assigned variable names are given in Table 7.

Table 7 – BMS Protocol Parameters

Parameter Name	Type	Description	Category
BCoolingActive	Boolean switch [-]	Pack cooling active indicator	Calculated
BLimpModeActive	Boolean switch [-]	Limp mode active indicator	Calculated
BOverCurrent	Boolean switch [-]	Pack over-current indicator	Calculated
BOverVoltage	Boolean switch [-]	Pack over-voltage indicator	Calculated
BPackBalanced	Boolean switch [-]	Pack balance status indicator	Calculated
BPowerWarning	Boolean switch [-]	Pack maximum power demand exceeded indicator	Calculated
BShutdownActive	Boolean switch [-]	Pack/vehicle shutdown switch	Calculated
BUnderSOC	Boolean switch [-]	Pack under minimum SOC indicator	Calculated
BUnderVoltage	Boolean switch [-]	Pack under minimum voltage indicator	Calculated
BVehicleOn	Boolean switch [-]	Vehicle on/off status indicator	Input
BVehicleStopped	Boolean switch [-]	Vehicle stopped/in motion indicator	Calculated
CBattery	Capacity [Ah, As]	Battery capacity	Stored
CCell	Capacity [Ah, As]	Cell capacity	Stored
CDischarged	Capacity [Ah, As]	Capacity discharged between time bounds	Calculated
IPack	Current [A]	Battery pack current draw	Input
IPack_Max_ActivateLimpMode	Current limit [A]	Battery pack upper limit; trigger limp mode	Stored
IPack_Max_ActivateShutdown	Current limit [A]	Battery pack upper limit; trigger shutdown	Stored
IPack_Min_ActivateShutdown	Boolean switch [-]	Battery pack charging current (-ve) limit; trigger shutdown	Stored
NCells	Integer [-]	Number of cells in battery	Stored
SOC_Min_ActivateLimpMode	SOC limit [%, -]	SOC Lower limit; trigger limp mode	Stored
SOC_Min_ActivateShutdown	SOC limit [%, -]	SOC Lower limit; trigger shutdown	Stored
TPack	Temperature [C]	Pack temperature	Input
TPack_Max_ActivateLimpMode	Temperature [C]	Pack temperature upper limit; trigger limp mode	Stored
TPack_Max_ActivateShutdown	Temperature [C]	Pack temperature upper limit; trigger shutdown	Stored
TPack_Min_ActivateLimpMode	Temperature [C]	Pack temperature lower limit; trigger limp mode	Stored
TPack_Min_ActivateShutdown	Temperature [C]	Pack temperature lower limit; trigger shutdown	Stored
tSample	Vector [s]	Sample time	Input
TTarget	Temperature [C]	Target/ideal operating temperature	Stored
vCarSample	Vector [m/s, kph]	Sample vehicle speed	Input
VCell	Voltage [V]	Cell voltage	Input
VCell_Max_ActivateLimpMode	Voltage limit [V]	Upper cell voltage limit; trigger limp mode	Stored
VCell_Max_ActivateShutdown	Voltage limit [V]	Upper cell voltage limit; trigger shutdown	Stored
VCell_Min_ActivateLimpMode	Voltage limit [V]	Lower cell voltage limit; trigger limp mode	Stored
VCell_Min_ActivateShutdown	Voltage limit [V]	Lower cell voltage limit; trigger shutdown	Stored
VPack	Voltage [V]	Pack voltage	Input

3.6.1 Pseudocode Protocol

A full ‘pseudocode’ version of the protocol is given in Appendix C. This attempts to describe all BMS functionality through a combination of MATLAB syntax code, mathematical notation and natural language commentary. Inside a functional system, this protocol would be evaluated reiteratively at constant frequency. Figure 23 and Figure 24 show example sections of the code.

```
function BMSProtocol = (InputDataChannels, StoredData)

% Determine if vehicle is active
BVehicleOn = InputDataChannels.BVehicleOn;

% Get current date/time
tSample    = InputDataChannels.tSample;

%Get current sampling frequency, Hz
fSample    = InputDataChannels.fSample;

% Calculate sampling period, s
pSample    = 1/fSample;

% If vehicle is inactive, return to low power consumption mode
if BVehicleOn == 0
    ActivateBMSSleepMode;
    return
end

% Otherwise, retrieve limits from StoredData
% Shutdown bounds
VCell_Max_ActivateShutdown = StoredData.VCell_Max_ActivateShutdown;
VCell_Min_ActivateShutdown = StoredData.VCell_Min_ActivateShutdown;
IPack_Max_ActivateShutdown = StoredData.IPack_Max_ActivateShutdown;
IPack_Min_ActivateShutdown = StoredData.IPack_Min_ActivateShutdown;
TPack_Max_ActivateShutdown = StoredData.TPack_Max_ActivateShutdown;
TPack_Min_ActivateShutdown = StoredData.TPack_Min_ActivateShutdown;
SOC_Min_ActivateShutdown   = StoredData.SOC_Min_ActivateShutdown;
```

Figure 23 - Psuedocode Protocol Example 1

```
% Step 5 - Calculate SOC
%-----------------------------------------------------------------
SOC = SOC_Previous - (C_Discharged/CBattery_Instantaneous);
```

Where this therefore satisfies;

$$SOC_{tSample} = SOC_{tSample-pSample} - \left(\frac{1}{C_{Instantaneous}} \cdot \int_{tSample-pSample}^{tSample} IPack \ \mathrm{dt}\right)$$

(See Eq. 4, pp. 12.)

```
% Write newly calculated SOC to logbook;
WriteToLogbook(SOC, tSample);
```

Figure 24 - Psuedocode Protocol Example 2

4 Further Work – Prototype Design

Also undertaken during the course of the project was the design of a complete scaled prototype that would be capable of effecting a basic version of the protocol described in 3.5.3 and Appendix C. The prototype design utilises six 14500 lithium-iron phosphate batteries in conjunction with a hall effect current sensor, a Linear Technology LTC6803 [33] battery monitor integrated circuit and a chipKIT Max32 [34] prototyping microcontroller. Figure 25 illustrates the structure of the prototype, whereby a battery monitor PCB would be produced, before being connected to both

the battery pack and the Max32. This monitor board would hold both the LTC6803 and the hall effect current sensor, as well as all necessary ancilliary components. Communication between the monitor board mounted LTC6803 and the Max32 could then take place via a Serial Peripheral Interface (SPI) bus.

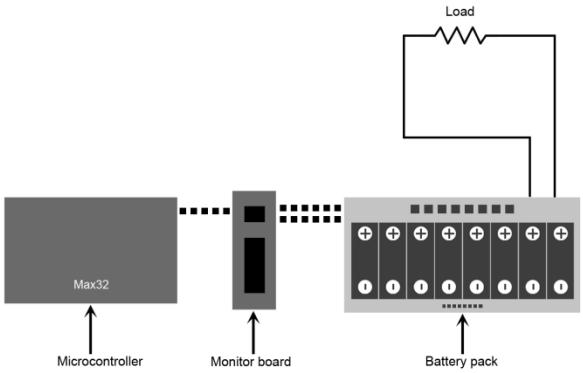

Figure 25 - Prototype Block Diagram

To enable drive cycle emulation, a digitally controlled potentiometer could then be used to control discharge current from the battery pack through a connected shunting load. This would permit scaled current demand profiles to be achieved by the prototype while the Max32 enacts the SOC and SOH calculation strategies given in 3.5.3 and Appendix C. Full prototype specification is given in Appendix D and a bill of quantities is given in Appendix E. Prototype schematics and PCB layout information are given in Appendix F.

5 Results

The outcomes of the described research may be divided into three distinct parts. The first is a completed and functional BMS protocol. The second is a completed software based vehicle simulation package that permits flexible BMS protocol development. The third is the output data provided by this simulation package when modelling an electric vehicle under set drive cycle conditions. This output data provides proof of protocol concept and functionality. It may also provide a method for comparing battery performance with manufacturer specifications.

5.1 BMS Protocol

As described in 3.6, a full psuedocode version of the developed protocol is given in Appendix C. This protocol is capable of executing safety and fault checks, monitoring battery states and correcting battery imbalance. Its effectiveness is discussed in 5.3.1 and 5.3.2.

5.2 Simulation Software Package

The simulation software package, as mentioned in 3.2, has many flexible, user controllable features. All input data, such as battery information files, battery logbook files and drive cycle

data, is stored in non-proprietary comma separated variable format. This facilitates the creation and editing of new simulation profiles without mandating that the software user have access to licenced copy of MATLAB; the tool may be compiled and deployed to any computer with the MATLAB Runtime Environment.

5.3 Simulation Output Data

When the software simulates a drive cycle, the various parameters described in 3.3 and 3.4 are calculated at each sample point. Accordingly, by reviewing the data generated during a simulation, it is possible to provide evidence of the developed protocol's efficacy and the simulation's validity. Output data may also form the basis for making comparisons with manufacturer provided battery specifications.

5.3.1 Evaluation of Protocol Operation and Simulation Effectiveness

For example, where the EPA UDDS [23] drive cycle is modelled for a vehicle of 1400kg kerb weight powered by a battery composed of 4000 (W50H80) Panasonic UPF476790 cells [31], the simulation package produces the output plots shown in Figure 26 .

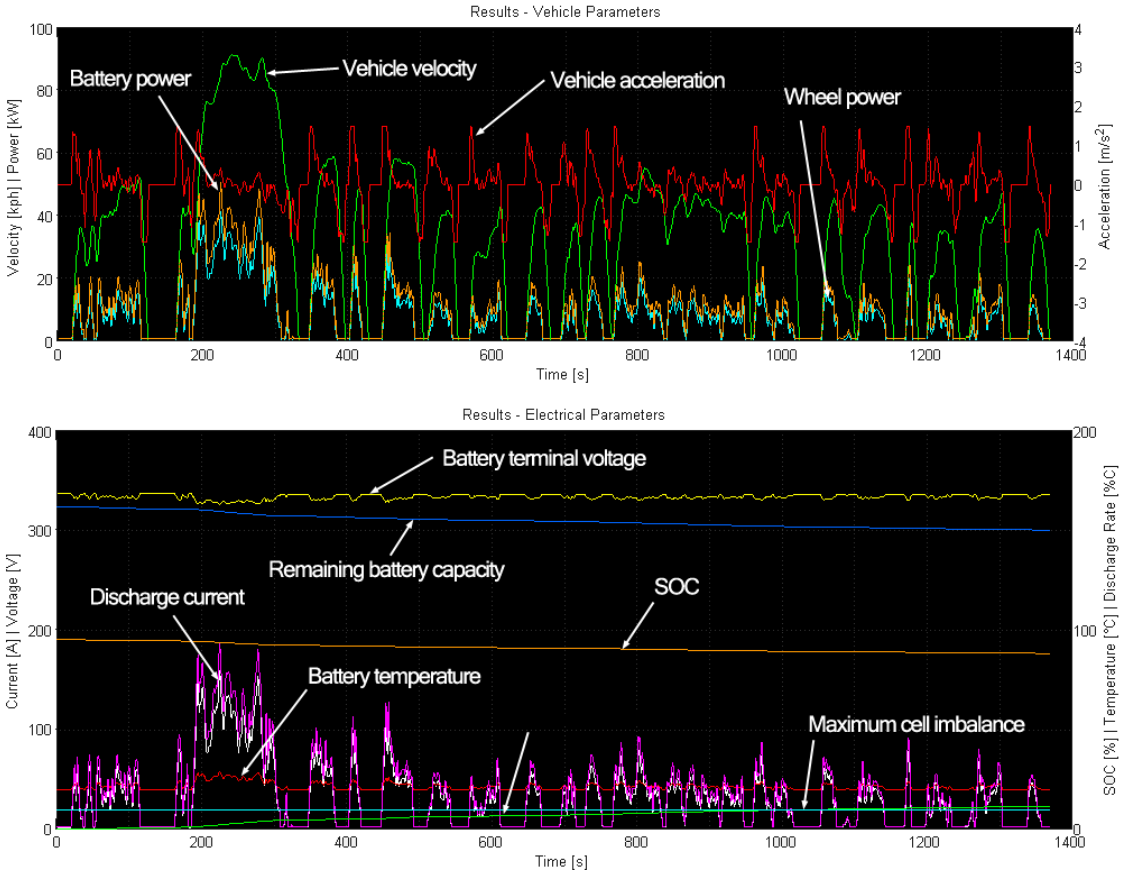

Figure 26 – UDDS Schedule – Protocol Overview

As Figure 26 shows, the BMS protocol calculates instantaneous SOC at every step in the drive cycle. During this schedule, no operating limits were breached and no shut down or limp

commands issued. Accordingly, the quantity of BMS information plotted is limited, though the line indicating maximum cell imbalance highlights the slow nature of the simulated dissipative balancing strategy. During the 1400s drive schedule, maximum imbalance is reduced by just 0.1%. Note that the tool's SOH calculations are made retrospectively following each drive cycle simulation, as they consider the entirety of the specified battery's logged history. In this case, as the battery was modelled as initially unused, SOH following drive cycle completion was reported as 99.9885%. Figure 26 also highlights simulation outputs, providing validation of the methods described in 3.3 and 3.4. In particular, it is possible to see substantial battery terminal voltage drop under high load. The discrepancy between battery pack power output and the power output required at the driven wheels also highlights power losses to drivetrain inefficiency and vehicle parasitic loads.

To simulate additional protocol features, the Boolean switches dictating which operational mode is to be used may be artificially thrown. For example, Figure 27 illustrates a simulated temperature sensor failure. At the point of simulated sensor failure, the vehicle's limp mode is activated, limiting available battery current and ultimately impacting available tractive effort and therefore achievable velocity.

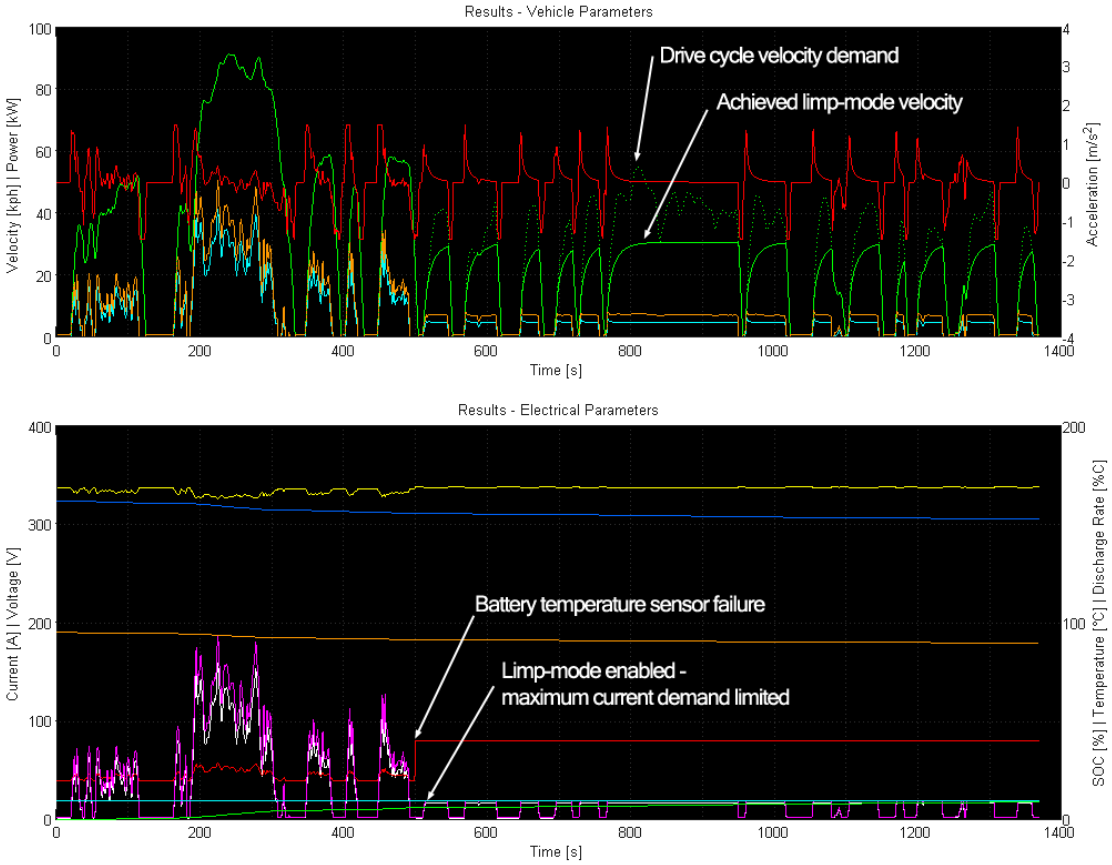

Figure 27 - UDDS Schedule - Simulated Sensor Failure

5.3.2 Evaluation of Logbooking Strategy and SOH Calculation

To evaluate the results of the enacted logbooking strategy, an unused battery of the 4000 cell Panasonic UPF476790 [31] format was simulated as the power source for a 1400kg vehicle completing five EPA FTP-75 [23] drive cycles without any charging. Cumulative data, binned appropriately, is shown in Figure 28.

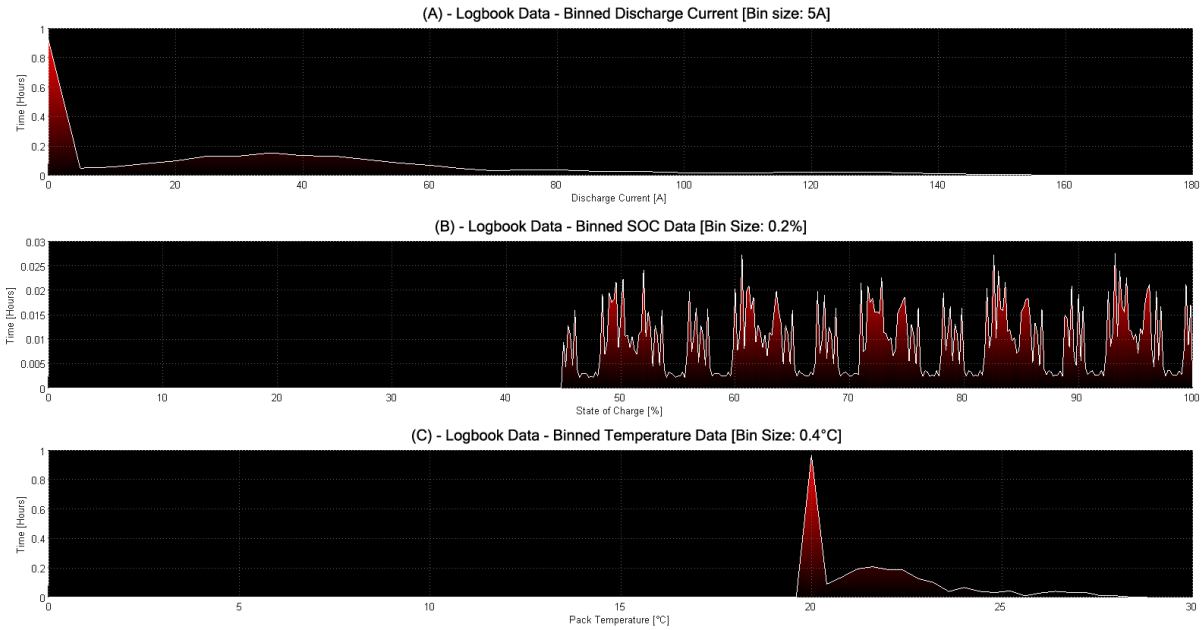

Figure 28 – Logbook Data

This data, when processed, indicated a SOH of 99.9211%.

5.3.3 Comparison with Manufacturer Specifications

Due to the lack of availability of true electric vehicle batteries on which characterising tests could be performed, the described simulation methods are strongly dependent on manufacturer provided data. As a result, there is a cyclical element to the modelling procedure, whereby output information is fundamentally dependent on input information. Therefore, attempts to compare modelled battery performance with manufacturer specifications are incapable of producing any unexpected results. The only valid exception to this is documented typical cell capacity.

Panasonic [31] state the typical cell capacity of the UPF476790 is 3400mAh, with rated minimum of 3280mAh. As they provide no data indicating the load conditions under which this capacity was measured, it becomes possible to investigate typical and minimum capacities under a number of drive cycles.

5.3.3.1 Average Cell Capacities under Differing Drive Cycles

To investigate fluctuations in cell capacity based on usage profile, a simulated run for new batteries discharging from 100% SOC to 0% SOC was completed with each of the four following drive cycles:

1. New European Drive Cycle (NEDC).
2. EPA FTP-75.
3. EPA UDDS.
4. EPA US06.

This was achieved by concatenating[†] multiple drive cycles and simulating these as one contiguous, enlarged schedule. This is shown in Figure 29, where a number of NEDC cycles have been combined. Note that only electrical parameters are shown. Also note the variation in pack current required to meet power demand arising from falling SOC and its effect on battery terminal voltage.

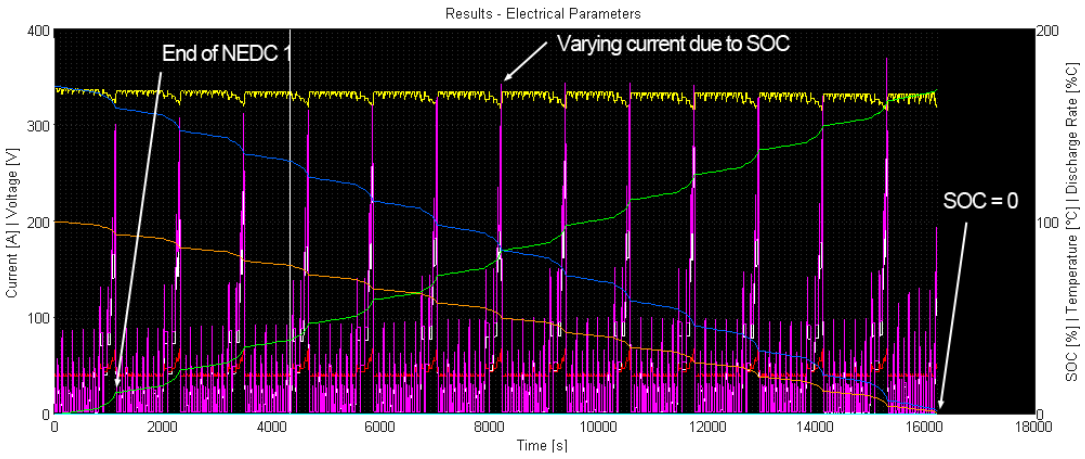

Figure 29 - NEDC Concatenated Drive Cycle

The average cell capacity for each of the four drive cycles is shown in Figure 30.

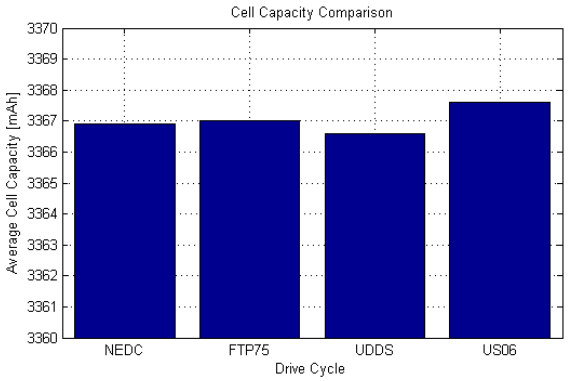

Figure 30 - Average Cell Capacities

[†] Concatenation refers to the end-to-end 'joining together' of data.

6 Discussion

6.1 BMS Protocol

The results shown in Figure 26 and Figure 27 confirm that the developed battery management protocol is functional and effective. It is capable of continually monitoring battery state via a highly flexible, easily translated interpolation based strategy that could be adapted to suit many real-world scenarios. In its operation, as shown in Figure 26, Figure 27 and Appendix C, the protocol provides multi-level safety and fault checking. It also offers a highly adaptive method for SOC calculation; continually evaluating and considering instantaneous battery capacity based on instantaneous operating conditions. SOH monitoring is also highly flexible, permitting high accuracy SOH calculations where suitable battery characterising data is available. Alongside its uses for SOH determination, the protocol's logbooking strategy, which records operating current, temperature and SOC, also permits accurate monitoring of battery charging times, currents and voltages. This capability offers the protocol the potential to be developed further to include charging control functionality.

However, the developed protocol is also vulnerable to issues with input data. For example, in Figure 28, where the logged data from a simulated battery powering five FTP-75 cycles is shown, SOH was reported as 99.9211%. At approximately half an hour per cycle, this would suggest around a 0.0316% drop in SOH for every hour of vehicle usage. Where a vehicle may be used for around ten hours per week, this would suggest around 15% deterioration in battery SOH over the course of an average year. This figure, the product of the 'placeholder' SOH strategy maps, is larger than that which could be expected from a real battery. Accordingly, accurate data is essential if the described SOH evaluation method is to be applied. Nevertheless, it is considered a valid proof of concept.

6.2 Simulation Software Package

The developed EV Sim Tool package acted as useful host in which the target BMS protocol could be developed and tested. Created with a high regard for the value of a 'user friendly' interface, EV Sim Tool may form the basis for future software based simulations conducted by the author. The intentional use of generic file formats also facilitates the translation of the developed protocol into an embeddable programming language such as C or C++ without the need for lengthy rewriting of file handling sections.

6.3 Simulation Output Data

6.3.1 Simulation Validation

The information displayed in Figure 26, Figure 27 and Figure 29 provides some degree of model validation. Both wheel and battery power figures are within the expected region for a vehicle of the simulated weight, whilst simulation response to reduced current handling capability suggests that the looped modelling approach is effective.

6.3.2 Comparison with Manufacturer Specifications

As described in 5.3.3, all battery input data during the simulation process is sourced from manufacturer specification. Therefore no unexpected results were produced. However, Figure 30 highlights cell capacity sensitivity to usage profile. During the EPA UDDS drive cycle average cell capacity is visibly less than during each of the other tested drive schedules. That said, the maximum deviation between simulated capacities was just 4mAh, 0.12% of manufacturer specified typical capacity. Each average capacity was also at least 386mAh above manufacturer rated minimum.

6.4 Comparison with Published and Existing Systems

The developed battery management protocol and associated battery state tracking methods share some similarities with commercially available battery management systems. However, many of these systems' manufacturers do not reveal their state tracking algorithms, so full comparisons are difficult to make. For example, Ashwoods [34] manufacture a modular battery management system which offers SOC, SOH and temperature monitoring, alongside user specifiable current limiting functionality. This approach has much in common with that developed, though Ashwoods state that SOH calculation is achieved by monitoring cell impedance rather than through a mapping based strategy such as that developed during the course of the project.

Investigation of published research shows that recent developments within academia have focused on 'intelligent' algorithms and more complex state tracking methods. For example, Wang [35] describes the development of a SOC tracking algorithm that utilises a 'learning' artificial neural network which may be trained via backward propagation of errors. Chen et al. [36] apply extended Kalman filter and artificial neural network methods to enable SOC estimation. These methods, which are adaptive and self-learning, are better able to respond to any unexpected battery operation phenomena than more simplistic map and current measurement based

estimation. Ultimately, the highly non-linear nature of battery behaviour may render these intelligent methods necessary for increased BMS performance.

However, with accurate characterising data and high accuracy measurement, a coulomb counting and interpolation based approach to state tracking still offers an effective means for battery management. In particular, investigation into published literature shows that the described methods for instantaneous SOC calculation and improved accuracy SOH tracking appear to feature novel additions to previously documented techniques.

7 Conclusions

The research undertaken provides one valid approach to electric vehicle battery management. More broadly, the full range of available battery management strategies serve to continually push electric vehicle technology forward, increasing electric vehicle performance and making them a more attractive proposition to consumers. However, when compared with more widely available internal combustion engine vehicles, it is apparent that electric vehicle technology still has many hurdles to overcome before it can be presented as a true alternative. Amongst these are the high initial cost for lithium-ion and lithium-polymer batteries, their long charging times and their short service life. Recent concerns over the safety of lithium-ion chemistry [37] also serve to damage public confidence in the technology.

That said, pressure from the environmental lobby is unrelenting, and the high level of efficiency and control afforded by powering a vehicle with electric motors makes them an attractive prospect for the next generation of automotive engineers. As a result, it seems likely that hybrid and fully electric vehicle technologies will only become more commonplace in the coming years.

7.1 Possible Future Research

The research conducted provides a useful basis for a number of possible future works. The MATLAB based software simulation package would permit the development of a more complex, adaptive battery management strategy such as those based upon neural networks or a fuzzy logic. Due to the way in which the software package was written, this system could be implemented within the existing EV Sim Tool framework without substantial re-writing required.

Equally, the included prototype designs, if assembled and tested, would permit evaluation of the existing battery management protocol. It may be the case that the novel additions to the lookup table based approach offer reasonable improvements to BMS performance and battery state tracking. This would be achieved at low cost and be easily commercialised if desired.

References

[1] Toyota. Prius. Toyota, Surrey, UK. [Online] Accessed 31st October 2013, available: http://www.toyota.co.uk/cgi-bin/toyota/bv/frame_start.jsp?id=CC2-Prius-landing

[2] Mercedes-AMG. The SLS AMG Coupé Electric Drive. Mercedes-AMG GmbH, Stuttgart, Germany. [Online] Accessed 31st October 2013, available: http://www.mercedes-amg.com/webspecial/sls_e-drive/eng.php

[3] Parliamentary Office of Science & Technology, "Electric Vehicles," *Postnote*, Number 365, October 2010. [Online] Accessed 31st October 2013, available: http://www.parliament.uk/documents/post/postpn365_electricvehicles.pdf

[4] Great Britain. Climate Change Act 2008: Elizabeth II. *Chapter 27, S. 1.* London, UK: H.M. Stationery Office, 2008. [Online] Accessed 31st October 2013, available: http://www.legislation.gov.uk/ukpga/2008/27/pdfs/ukpga_20080027_en.pdf

[5] SMMT (2013, Jan). December 2012 – EV and AFV registrations. SMMT, London, UK. [Online] Accessed 31st October 2013, available: http://www.smmt.co.uk/2013/01/december-2012-%E2%80%93-ev-and-afv-registrations/

[6] D. Sandalow, *Plug-in Electric Vehicles – What Role for Washington?,* Washington, DC, USA: Brookings Institution Press, 2009, pp. 2.

[7] C. Chan, "The State of the Art of Electric, Hybrid and Fuel Cell Vehicles," *Proc. IEEE*, vol. 95, pp. 704 – 718, April 2007.

[8] I. Husain, *Electric and Hybrid Vehicles: Design Fundamentals*, Boca Raton, Florida, USA: CRC Press, 2003.

[9] C. Rahn and C. Wang, *Battery Systems Engineering*, West Sussex, UK: Wiley, 2013.

[10] G. Pistoia, *Electric and Hybrid Vehicles*, Amsterdam, NL: Elsevier, 2010.

[11] J. Larminie and J. Lowry, *Electric Vehicle Technology Explained*, West Sussex, UK: Wiley, 2003.

[12] D. Reisner and M. Klein, "Bipolar Nickel-Metal Hydride Battery for Hybrid Vehicles," in *Battery Conference on Applications and Advances*, *Proc. 9th Annu.*, 1994, pp. 111 – 116.

[13] X. Chen et al., "An Overview of Lithium-Ion Batteries for Electric Vehicles," in *IPEC 2012 Conf. on Power & Energy,* 2012, pp. 230 – 235.

[14] A. Hoke et al., "Maximizing Lithium Ion Vehicle Battery Life Through Optimized Partial Charging," in *Innovative Smart Grid Technologies (ISGT), 2013 IEEE PES*, 2013, pp. 1 – 5.

[15] H. Venkatasetty and Y. Jeong, "Recent Advances in Lithium-Ion and Lithium-Polymer Batteries," in *Battery Conf. on Applications and Advances, Proc. 17th Annu.*, 2002, pp. 173 – 178.

[16] V. Pop et al., *Battery Management Systems – Accurate State-of-Charge Indication for Battery-Powered Applications*, New York, NY, USA: Springer, 2008.

[17] S. Piller et al., "Methods for state-of-charge determination and their applications," *Journal of Power Sources*, Vol. 96, 2001, pp.113 – 120.

[18] K. Soon Ng et al., "Enhanced coulomb counting method for estimating state-of-charge and state-of-health of lithium-ion batteries," *Applied Energy,* Vol. 86, 2009, pp. 1506 – 1511.

[19] S. Wen, "Cell balancing buys extra run time and battery life," *Texas Instruments Analog Applications Journal*, Q1 2009, pp. 14 – 18, 2009.

[20] M. Daowd et al., "Passive and active battery balancing comparison based on MATLAB simulation," in *IEEE Vehicle Power and Propulsion Conf. (VPCC)*, 2011, pp. 1 – 7.

[21] J. Cao et al., "Battery Balancing Methods: A Comprehensive Review," in *IEEE Vehicle Power and Propulsion Conf. (VPCC),* 2008, pp. 1 – 6.

[22] M. Daowd et al., "A Review of Passive and Active Battery Balancing based on MATLAB/Simulink," unpublished.

[23] EPA. Dynamometer Drive Schedules. United States Environmental Protection Agency: National Vehicle & Fuel Emissions Laboratory, Michigan, USA. [Online] Accessed 27th March 2014, available: http://www.epa.gov/nvfel/testing/dynamometer.htm

[24] T. Barlow et al., *A reference book of driving cycles for use in the measurement of road vehicle emissions*, Berkshire, United Kingdom: Transport Research Laboratory, 2009. [Online] Accessed 19th March 2014, available: https://www.gov.uk/government/uploads/system/uploads/attachment_data/file/4247/ppr-354.pdf

[25] BMW. BMW 3 Series Sedan Technical Data, BMW AG, Munich, Germany. [Online] Accessed 19th March 2014, available: http://www.bmw.com/com/en/newvehicles/3series/sedan/2008/allfacts/engine/technical_data.html

[26] The Mayfield Company. Index to Coefficient of Drag for Many Vehicles Plus Index to Horsepower vs. Speed Curves. Mayfield Motorsports, USA. [Online] Accessed 19th March 2014, available: http://www.mayfco.com/tbls.htm

[27] *Stepwise Coastdown Methodology for Measuring Tire Rolling Resistance,* SAE Standard J2452, 1999.

[28] MathWorks. Documentation Center – Rolling Resistance. The MathWorks, Inc., Massachusetts, USA. [Online] Accessed 28th March 2014, available: http://www.mathworks.co.uk/help/physmod/sdl/ref/rollingresistance.html

[29] M. Knauff et al., "Simulink Model of a Lithium-Ion Battery for the Hybrid Power System Testbed," in *IEEE Electric Ship Technologies Symp.,* 2007, pp. unknown.

[30] M. Gholizadeh, F. Salmasi, *"Estimation of State of Charge, Unknown Nonlinearities, and State of Health of Lithium-Ion Battery Based on a Comprehensive Unobservable Model,"* in *IEEE Trans. Ind. Electron.,* Vol. 61, 2014, pp. 1335 – 1344.

[31] Panasonic. Lithium-Ion: Make your product Powered by Panasonic. Panasonic Corporation of North America, New Jersey, USA. [Online] Accessed March 29th 2014, available: http://www.panasonic.com/industrial/batteries-oem/oem/lithium-ion.aspx

[32] Nissan Global. Electric Vehicle Lithium-ion Battery. Nissan Motor Co., Yokohama, Japan. [Online] Accessed March 29th 2014, available: http://www.nissan-global.com/EN/TECHNOLOGY/OVERVIEW/li_ion_ev.html

[33] Linear Technology. LTC6803-1 and -3 – Multicell Battery Stack Monitor. Linear Technology Corporation, California, USA. [Online] Accessed 31st March 2014, available: http://www.linear.com/product/LTC6803-1

[34] Digilent. chipKit Max32 Prototyping Platform. Digilent Incorporated, Washington, USA. [Online] Accessed 31st March 2014, available: https://digilentinc.com/Products/Detail.cfm?NavPath=2,892,894&Prod=CHIPKIT-MAX32

[35] C. Weng, *"Prediction of Battery SOC of Pure Electric Vehicle,"* in *Int. Conf. on Computer Science & Education*, *Proc. 7th Annu.*, 2012, pp. 466 – 469.

[36] Z. Chen et al., *"Battery State of Charge Estimation Based on a Combined Model of Extended Kalman Filter and Neural Networks",* in *Proc. Int. Joint Conf. on Neural Networks*, 2011, pp. 2156 – 2163.

[37] Mark Gregory. Boeing 787: Dreamliner's lithium ion batteries probed. BBC News, London, United Kingdom. [Online] Accessed 31st March 2014, available: http://www.bbc.co.uk/news/business-21059605

Appendix A – Project Management

Work Plan

Error! Reference source not found. illustrates the project's planned structure.

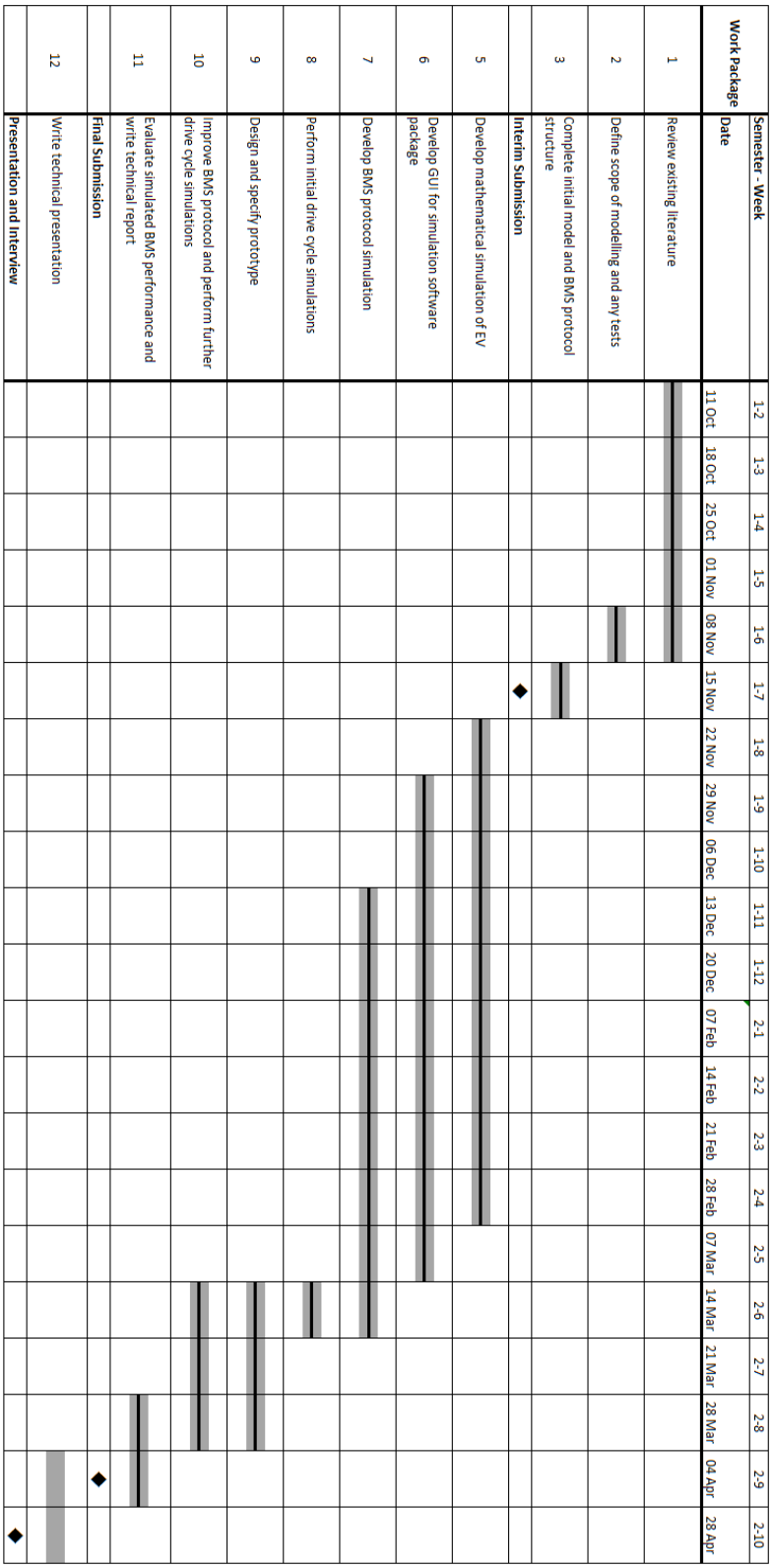

App. A - Figure 1 - Project Plan

Appendix B – EV Sim Tool User Interface

This section gives some example images of the developed software package's user interface and operation.

App. B - Figure 1 – EV Sim Tool 'Splash Screen'

App. B - Figure 2 - EV Sim Tool 'Battery Pack' Setup

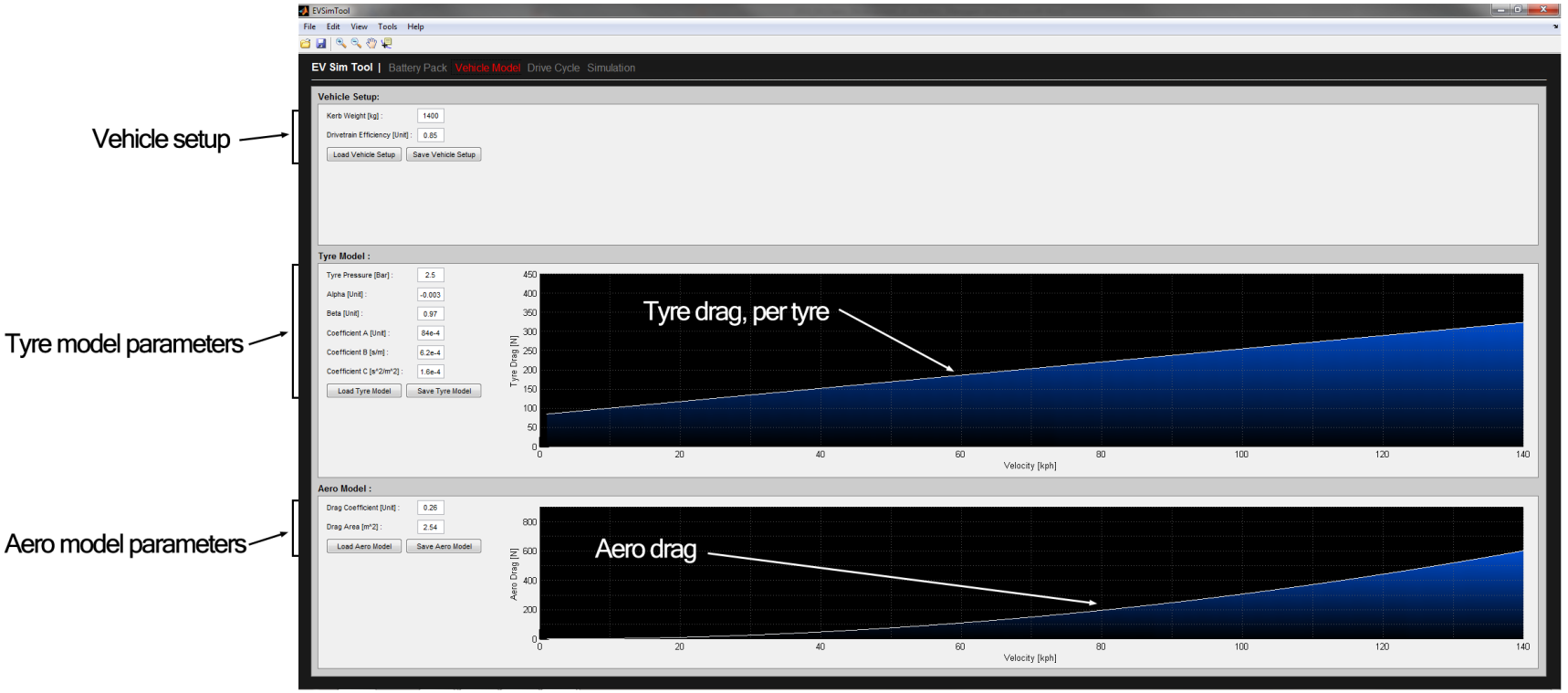
Active configuration tab: Vehicle Model
Specify vehicle modelling parameters
Vehicle setup
Tyre model parameters
Aero model parameters
EVSimTool
File Edit View Tools Help
EV Sim Tool | Battery Pack Vehicle Model Drive Cycle Simulation
Vehicle Setup:
Kerb Weight [kg] : 1400
Drivetrain Efficiency [Unit] : 0.85
Load Vehicle Setup
Save Vehicle Setup
Tyre Model :
Tyre Pressure [Bar] : 2.5
Alpha [Unit] : -0.003
Beta [Unit] : 0.97
Coefficient A [Unit] : 84e-4
Coefficient B [s/m] : 6.2e-4
Coefficient C [s^2/m^2] : 1.6e-4
Load Tyre Model
Save Tyre Model
Tyre drag, per tyre
Tyre Drag [N]
Velocity [kph]
Aero Model :
Drag Coefficient [Unit] : 0.26
Drag Area [m^2] : 2.54
Load Aero Model
Save Aero Model
Aero drag
Aero Drag [N]
Velocity [kph]

Active configuration tab: Drive Cycle

Specify simulation drive cycle

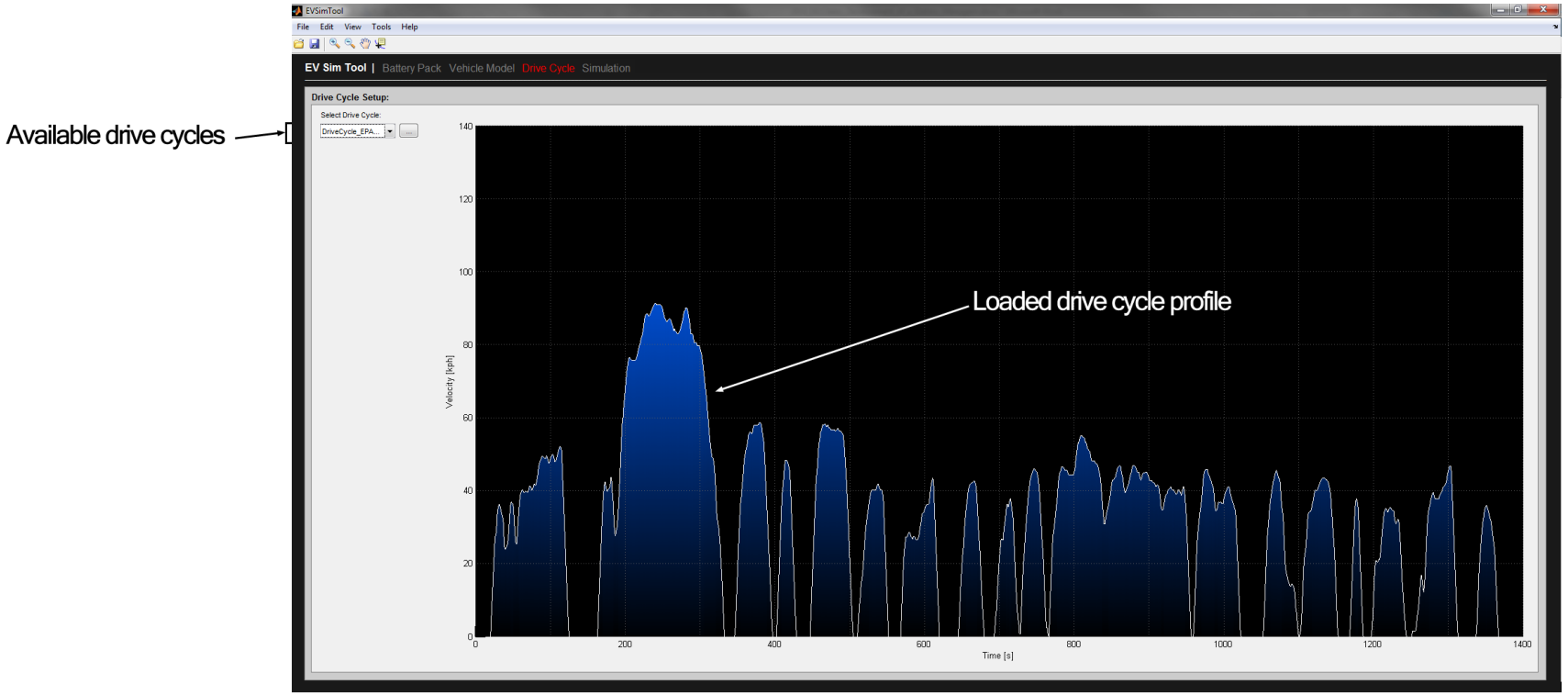

App. B - Figure 4 - EV Sim Tool 'Drive Cycle' Setup

Active configuration tab: Simulation

Run simulation and review output data

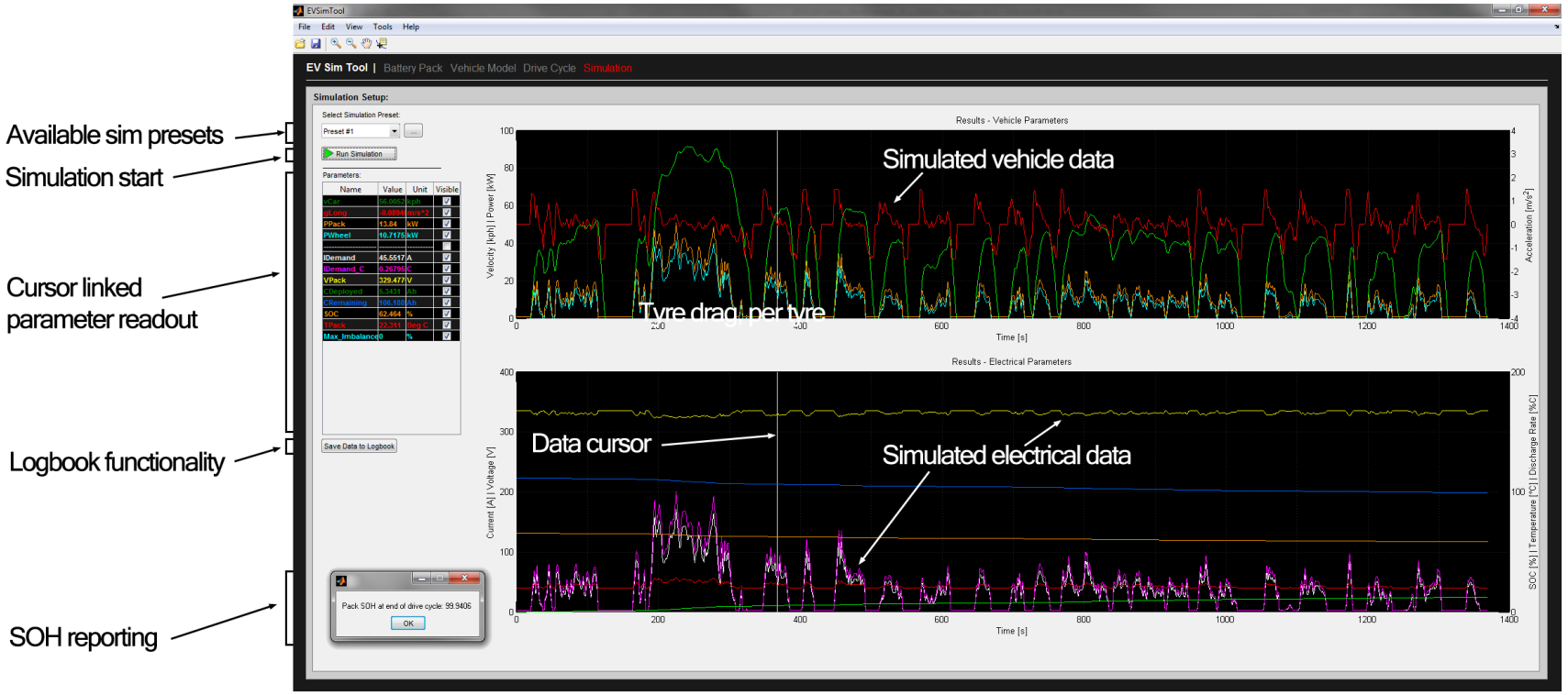

App. B - Figure 5 - EV Sim Tool 'Simulation'

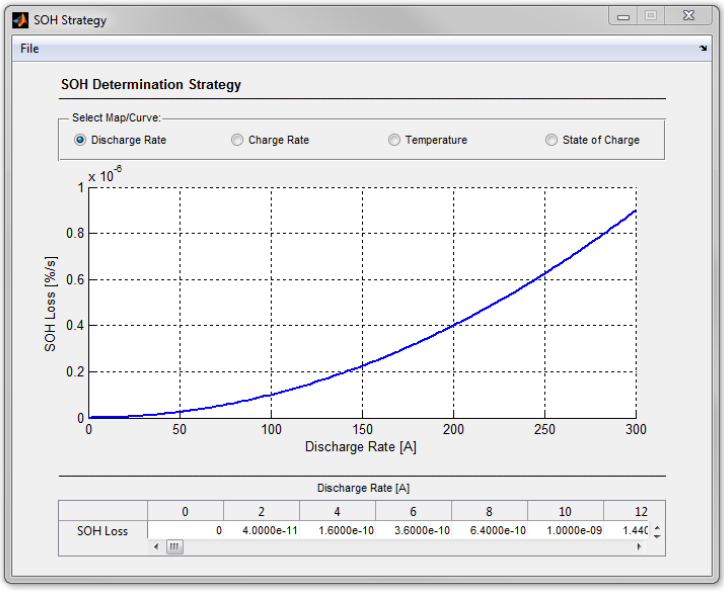

App. B - Figure 6 - EV Sim Tool SOH Strategy Viewer

Appendix C – Pseudocode Protocol

Notes on function inputs:

'InputDataChannels' represents all live input parameters to the BMS protocol. These are accessed using '.' notation, e.g., 'InputDataChannels.TPack' will return battery pack temperature information from the current round of input sampling. 'StoredData' represents all information available to the protocol from the system's memory. This includes all limits and lookup tables; though 'logbooking' information would also be stored in system memory.

Protocol Start

```
function BMSProtocol = (InputDataChannels, StoredData)

% Determine if vehicle is active
BVehicleOn = InputDataChannels.BVehicleOn;

% Get current date/time
tSample    = InputDataChannels.tSample;

%Get current sampling frequency, Hz
fSample    = InputDataChannels.fSample;

% Calculate sampling period, s
pSample    = 1/fSample;

% If vehicle is inactive, return to low power consumption mode
if BVehicleOn == 0
    ActivateBMSSleepMode;
    return
end

% Otherwise, retrieve limits from StoredData
% Shutdown bounds
VCell_Max_ActivateShutdown = StoredData.VCell_Max_ActivateShutdown;
VCell_Min_ActivateShutdown = StoredData.VCell_Min_ActivateShutdown;
IPack_Max_ActivateShutdown = StoredData.IPack_Max_ActivateShutdown;
IPack_Min_ActivateShutdown = StoredData.IPack_Min_ActivateShutdown;
TPack_Max_ActivateShutdown = StoredData.TPack_Max_ActivateShutdown;
TPack_Min_ActivateShutdown = StoredData.TPack_Min_ActivateShutdown;
SOC_Min_ActivateShutdown   = StoredData.SOC_Min_ActivateShutdown;


% Limp mode bounds
VCell_Max_ActivateLimpMode = StoredData.VCell_Max_ActivateLimpMode;
VCell_Min_ActivateLimpMode = StoredData.VCell_Min_ActivateLimpMode;
IPack_Max_ActivateLimpMode = StoredData.IPack_Max_ActivateLimpMode;
TPack_Max_ActivateLimpMode = StoredData.TPack_Max_ActivateLimpMode;
TPack_Min_ActivateLimpMode = StoredData.TPack_Min_ActivateLimpMode;
SOC_Min_ActivateLimpMode   = StoredData.SOC_Min_ActivateLimpMode;
```

```
% Get target/ideal operating temperature
TTarget = StoredData.TPackTarget;

% As vehicle is active, query all safety releveant parameters in
% the following order;
VCell_Values = InputDataChannels.VCell; %Corrected for series position &
transients
IPack = InputDataChannels.IPack; %Includes all load sources
TPack        = InputDataChannels.TPack;
vCarSample   = InputData.vCarSample;

% Determine if battery pack is being charged or discharged - employ sign
% convention
if IPack < 0
    % Determine if charging is happening while in motion, i.e. regeneration
    % /energy recovery is active
    if max(abs(vCarSample)) > 0.5
        %Regenerative switch
        BCharging_Regenerative = 1;
    else
        %Static, plugged in switch
        BCharging_Static = 1;
    end

    %Write to logbook
    WriteToLogbook(I_Charging, tSample, IPack);


else
    %Discharging switch
    BDischarging = 1;

    %Write to logbook
    WriteToLogbook(I_Discharging, tSample, IPack);
end


% Compare above parameters with safe operating limits, throw shutdown or
% limp switch if not - issue warning to user. Applies to discharging and
% energy recovery/regeneration conditions
if BDischarging == 1 | BCharging_Regenerative == 1
    if max(VCell_Values) > VCell_Max_ActivateShutdown
        BShutdown = 1;
        Warning = ('Warning - extreme over voltage condition. Vehicle
disabled.');
        disp(Warning)
    elseif min(VCell_Values) < VCell_Min_ActivateShutdown;
        BShutdown = 1;
        Warning = ('Warning - extreme under voltage condition. Vehicle
disabled.');
```

```
        disp(Warning)
    elseif max(IPack) > IPack_Max_ActivateShutdown;
        BShutdown = 1;
        Warning = ('Warning - extreme over current condition. Vehicle
disabled.');
        disp(Warning)
    elseif max(TPack) > TPack_Max_ActivateShutdown
        Warning = ('Warning - extreme over temperature condition. Vehicle
disabled.');
        disp(Warning)
        IncreaseCooling(TTarget);
    end

    if max(VCell_Values) > VCell_Max_ActivateLimpMode
        BLimpMode = 1;
        Warning = ('Warning - extreme over voltage condition. Limp mode
activated.');
        disp(Warning)
    elseif min(VCell_Values) < VCell_Min_ActivateLimpMode;
        BLimpMode = 1;
        Warning = ('Warning - extreme under voltage condition. Limp mode
activated.');
        disp(Warning)
    elseif IPack > IPack_Max_ActivateLimpMode;
        BLimpMode = 1;
        Warning = ('Warning - extreme over current condition. Limp mode
activated.');
        disp(Warning)
    elseif TPack > TPack_Max_ActivateLimpMode
        Warning = ('Warning - extreme over temperature condition. Limp mode
activated.');
        disp(Warning)
        IncreaseCooling(TTarget);
    end
end

% Compare above parameters with safe operating limits, throw shutdown
% switch if not - issue warning to user. Static charging only
if BCharging_Static == 1
    %As all values are -ve in sign, use min and < comparators
    if min(IPack) < IPack_Min_ActivateShutdown
        BShutdown = 1;
        Warning = ('Warning - charging current limit exceeded. System disabled');
        disp(Warning);
    elseif max(TPack) > TPack_Max_ActivateLimpMode %Use lower temperature limit
        Warning = ('Warning - extreme over temperature condition. System
disabled.');
        disp(Warning)
        IncreaseCooling(TTarget);
    end
end
```

```
% Account for shutdown switch position
if BShutdown == 1

    % Issue shutdown command - use 'Warning' to determine shutdown type
    ShutdownVehicle(Warning);

    % Record incident, time it occured and warning issued
    WriteToLogbook(Shutdown, tSample, Warning);
end

% Account for limp mode switch position
if BLimpMode == 1

    % Issue limp mode command  - use 'Warning' to determine limp mode type
    ActivateLimpMode(Warning);

    % Record incident, time it occured and warning issued
    WriteToLogbook(LimpMode, tSample, Warning);
end
```

If no shutdown/limp error is issued, begin data processing

```
% Step 1 - Retrieve SOC value from previous sampling event
%-----------------------------------------------------------------
SOC_Previous = GetFromLogbook(SOC, tSample-pSample);
```

$Where;$

$tSample(i-1) = tSample(i) - pSample.$

$And;\ \ pSample = sampling\ period\ in\ seconds.$

```
% Step 2 - Retrieve current draw at previous sampling event
%-----------------------------------------------------------------
IPack_Previous = GetFromLogbook(IPack, tSample-pSample);
```

```
% Step 3 - Calculate charge released since last sampling event
%-----------------------------------------------------------------
% Time step, dt
dt = pSample;

% Integrate using trapezoidal rule
```

```
C_Discharged = integrate_numerical([IPack_Previous, IPack], dt);

% Convert to Ah (fSample*60 = samples per hour)
C_Discharged = CapacityDischarged/(fSample*60);
```

$Where \quad integrate\_numerical([IPack\_Previous,\ IPack],\ dt) \quad performs\ the\ trapezoidal\ rule\ as\ follows;$

$$\int_{tSample-pSample}^{tSample} IPack\ \mathrm{dt} \approx \mathrm{dt} \cdot \left(\frac{IPack + IPack\_Previous}{2}\right)$$

```
% Step 4 - Calculate instantaneous capacity at current operating condition
%-----------------------------------------------------------------
% Get stored 2D table of instantaneous capacity vs temperature and current
CapacityMap = StoredData.CapacityMap;

% Interpolate through
CBattery_Instantaneous = Lookup2D(CapacityMap, IPack, TPack);

% Notes:
% - CBattery_Instantaneous represents the available capacity [Ah]
%   to cut-off voltage at specified temperature and discharge rate.
%   Its value is indicative of 100% SOC capacity at that condition.
%
% - This section operates with a one sample lag on SOC parameter
```

```
% Step 5 - Calculate SOC
%-----------------------------------------------------------------
SOC = SOC_Previous - (C_Discharged/CBattery_Instantaneous);
```

$Where\ this\ therefore\ satisfies;$

$$SOC_{tSample} = SOC_{tSample-pSample} - \left(\frac{1}{C_{Instantaneous}} \cdot \int_{tSample-pSample}^{tSample} IPack\ \mathrm{dt}\right)$$

$(See\ Eq.\ 4,\ pp.\ 12.)$

```
% Write newly calculated SOC to logbook;
WriteToLogbook(SOC, tSample);
```

```
% Step 6 - Begin balancing - vehicle must be stationary
%-----------------------------------------------------------------
%Determine if vehicle is stopped
if max(vCarSample) < 0.5 & min(vCarSample) > -0.5
```

```
    BVehicleStopped = 1;
end

if BVehicleStopped == 1

    %Check if battery pack is balanced
    %-----------------------------------------------------------------
    % Identify cells with highest voltages - corrected for their series
    % position & any transient effects - indicative of highest SOC
    [MaxCellVoltage, MaxVCellIndex] = max(VCell_Values);

    % Identify cells with lowest voltages - corrected for their series
    % position & any transient effects - indicative of lowest SOC
    [MinCellVoltage, MinVCellIndex] = min(VCell_Values);

    %Check balance, permit 1% voltage delta
    if MaxCellVoltage/MinCellVoltage < 1.01

        %Balanced
        BPackBalanced = 1;

    else

    %For cell-to-pack or dissipative balancing - issue balance command
    %---------------------------------------
    BalanceBattery(BalancingMethod, MaxVCellIndex);

    %For pack-to-cell balancing - issue balance command
    %---------------------------------------
    BalanceBattery(MinVCellIndex);

    %Notes:
    % Balancing current will now register >0A at the next round of
    % sampling, i.e. when tSample = tSample + pSample

    end

end
```

```
% Step 7 - Determine battery SOH effect - cycle count based
%-----------------------------------------------------------------
% Find cycle count - use manufacturer specified capacity as reference
CBattery_Specified = StoredData.CBattery_Specified;

% Get all historic current draw data
IPack_All = GetFromLogbook(IPack, t0:tSample);
```

```
% Integrate using reiterative trapezoidal rule
C_Discharged_Total = integrate_numerical(IPack_All, (0:tSample));
```

$Where \quad integrate\_numerical(IPack\_All, (0:tSample)) \quad performs\ the\ trapezoidal\ rule\ as\ follows;$

$$\int_{t0}^{tSample} IPack\ \mathrm{d}t \approx \sum_{i=t0}^{tSample-pSample} \left[\mathrm{d}t \cdot \left(\frac{IPack(i) + IPack(i+1)}{2}\right)\right]$$

```
% Convert to Ah (fSample*60 = samples per hour)
C_Discharged_Total = CapacityDischarged/(fSample*60);

% Calculate rounded number of cycles
nCyclesCompleted = round(C_Discharged_Total/CBattery_Specified);

% Get stored 1D table of long term capacity v cycle count
CycleLifeCurve = StoredData.CycleLifeCurve;

% Interpolate through to find long term capacity
CBattery_Cycles = Lookup1D(CycleLifeCurve, nCyclesCompleted);

% Find cycle dependent SOH - in %
SOH_Cycles = (CBattery_Cycles/CBattery_Specified)*100;
```

```
% Step 8 - Determine battery SOH - response map based
%-----------------------------------------------------------------
% Get discharge rate based info
DischargeRate_SOHCurve = StoredData.DischargeRate_SOHCurve;

% Get historic binned current craw
IPack_Binned = bin(IPack_All, BinBounds);



% Get temperature based info
Temperature_SOHCurve = StoredData.Temperature_SOHCurve;

% Get all historic temperature data
TPack_All = GetFromLogbook(TPack, t0:tSample);

% Get historic binned temperature data
TPack_Binned = bin(TPack_All, BinBounds);


% Get SOC based info
SOC_SOHCurve = StoredData.SOC_SOHCurve;

% Get all historic SOC data
```

```
SOC_All = GetFromLogbook(SOC, t0:tSample);

% Get historic binned SOC data
SOC_Binned = bin(SOC_All, BinBounds);


% Get losses
for i = 1:length(IPack_Binned)
    %Discharge rate
    SOHLoss_I = Lookup1D(DischargeRate_SOHCurve, IPack_Binned(i));

    %Temperature
    SOHLoss_T = Lookup1D(Temperature_SOHCurve, TPack_Binned(i));

    %SOC
    SOHLoss_SOC = Lookup1D(Temperature_SOHCurve, SOC_Binned(i));
end

% Get calendar loss
BatteryAge = GetFromLogbook(BatteryAge);

% 1% PA loss
SOHLoss_Calendar = BatteryAge*1;


% Add losses
SOHLoss_Total = SOHLoss_I + SOHLoss_T + SOHLoss_SOC + SOHLoss_Calendar;

% As SOH loss is already in %, calcualte total SOH
SOH_Pack = SOH_Cycles - SOHLoss_Total;
```

```
% Step 8 - Report
%-----------------------------------------------------------------------
ReportToUser(SOC, SOH_Pack);
```

Appendix D – Full Prototype Specification

Appendix E – Prototype Bill of Quantities

Item No.	Item Description	Item	Supplier	Stock No. / Order Code	Hyperlink	Rate Excl VAT	Rate Incl VAT	Quantity	Cost Excl VAT	Cost Inc VAT	Shipping & Handling
1	Battery charger	SKYRC T7655 Balance Charger	Amazon UK (Vendor: SKYRC)	N/A	T6755 Charger	£53.00	£63.60	1	£53.00	£63.60	£0.00
2	Microcontroller	chipKIT Max32 Development Board	RS Components	737-7950	Max32	£38.50	£46.20	1	£38.50	£46.20	£0.00
3	SD card module	Arduino Wireless Shield with SD socket	RS Components	748-5348	SD card module	£12.22	£14.66	1	£12.22	£14.66	£0.00
4	Battery monitor IC	Linear Technology LTC6803IG-3#PBF (Ships from USA)	Farnell	2308604	LTC6803	£20.34	£24.41	1	£20.34	£24.41	£15.95
5	Battery clips/terminals	Keystone AA Battery Clips (Pk 5)	Farnell	908733	AA Battery Clips	£1.00	£1.20	4	£4.00	£4.80	£0.00
6	Hall effect current sensor	Allegro Microsystems ACS712ELCTR-20A-T (SENSOR, CURRENT, 20A, SOIC8)	Farnell	1339624	ACS712ELCTR-20A-T	£3.41	£4.09	2	£6.82	£8.18	£0.00
7	Thermistor	EPCOS - B57164K104J - THERMISTOR, NTC	Farnell	9753443	Thermistor	£0.63	£0.76	10	£6.30	£7.56	£0.00
8	Terminal block	TE Connectivity - 1586037 - Header, Vertical, 2 row, 10 way, 4.2mm	Farnell	8115729	Terminal Block	£0.53	£0.64	3	£1.59	£1.91	£0.00
9	Terminal receptacle	TE Connectivity - 1-794954 - Housing, Receptacle, 2 row, 10 way, Nylon	Farnell	8115842	Terminal Receptacle	£0.22	£0.27	3	£0.66	£0.80	£0.00
10	Digital potentiometer	ANALOG DEVICES - AD7376ARUZ50	Farnell	2377009	AD Dig-Pot	£4.88	£5.86	2	£9.76	£11.71	£0.00
11	P Channel MOSFET	VISHAY SILICONIX - SI2307BDS-T1-E3 - P CH MOSFET	Farnell	1837452	P MOSFET	£0.37	£0.44	10	£3.66	£4.39	£0.00
12	Lithium ion batteries	3.2V AA 14500 Li-ion / LiFePO4 400mAh	Batteries Plus	N/A	Lithium ion batteries (AA/14500)	£3.25	£3.90	12	£39.00	£46.80	Not yet known
								TOTAL:	£195.85	£235.02	£15.95
										NET TOTAL:	£250.97

App. E - Figure 1 - Prototype Bill of Quantities

Appendix F – Prototype Schematics and PCB Layout

Final prototype specification uses the LTC6803's on-board MOSFETs for dissipative balancing. Accordingly no external MOSFETs are required. A schematic of the designed monitor board is given in App. F - Figure 1.

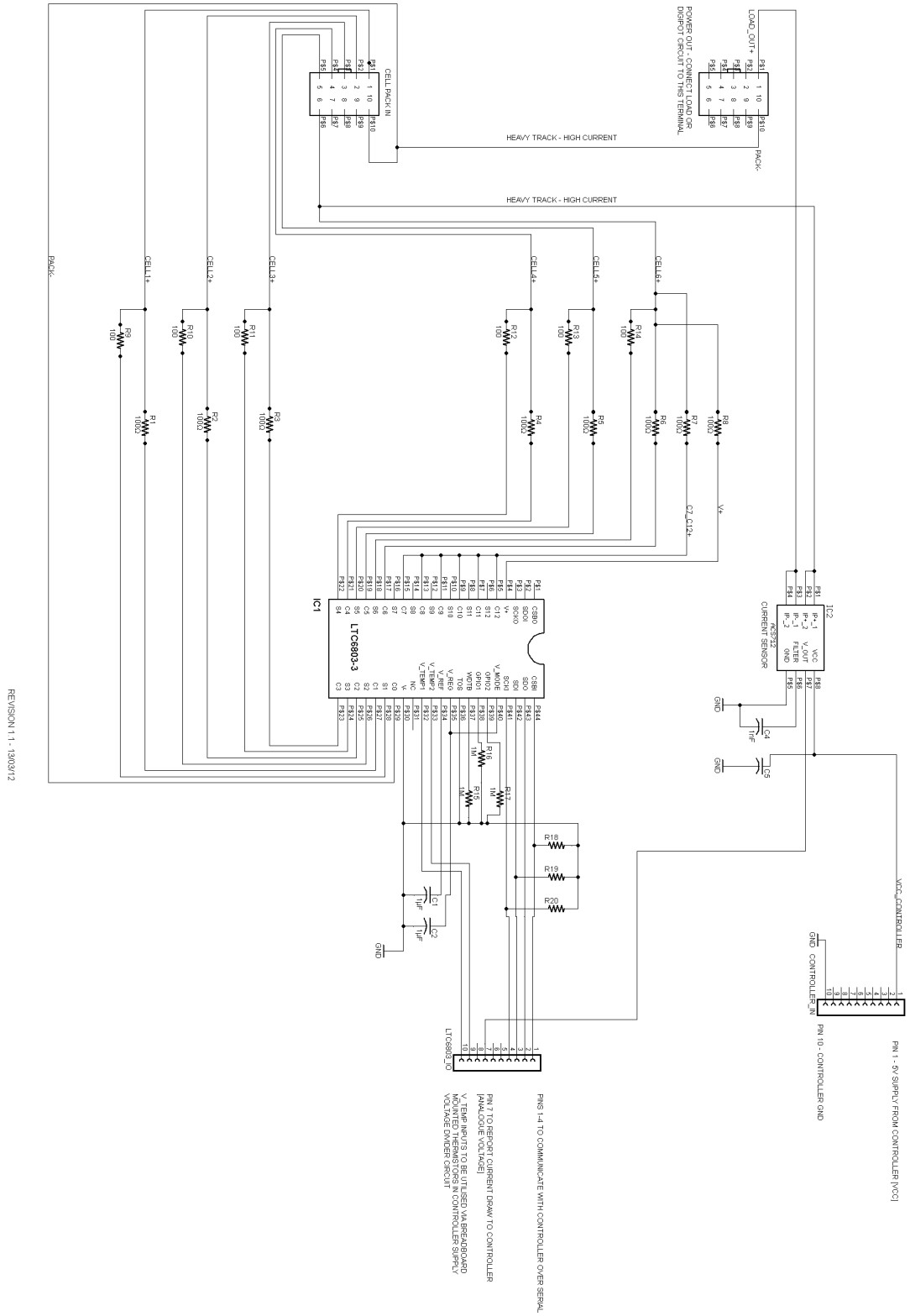

App. F - Figure 1 - System Schematic

A schematic of the designed discharge circuit is also given. This circuit would permit drive cycle emulation through scaled ‘replay’ of current demand profiles generated by EV Sim Tool. This is shown in App. F - Figure 2.

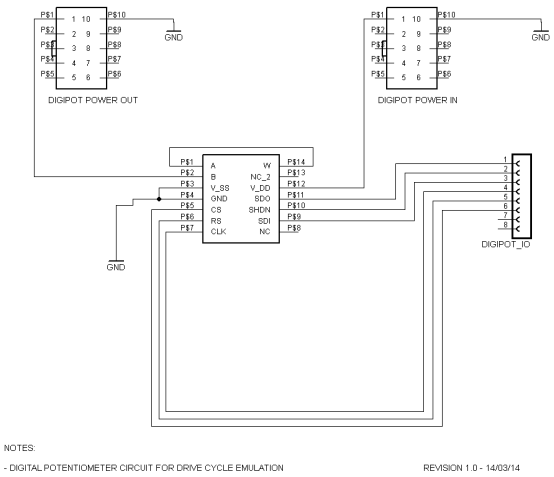

App. F - Figure 2 - Digital Potentiometer Circuit Schematic

A PCB layout was also created for the system shown in App. F - Figure 1. This is shown in App. F - Figure 3.

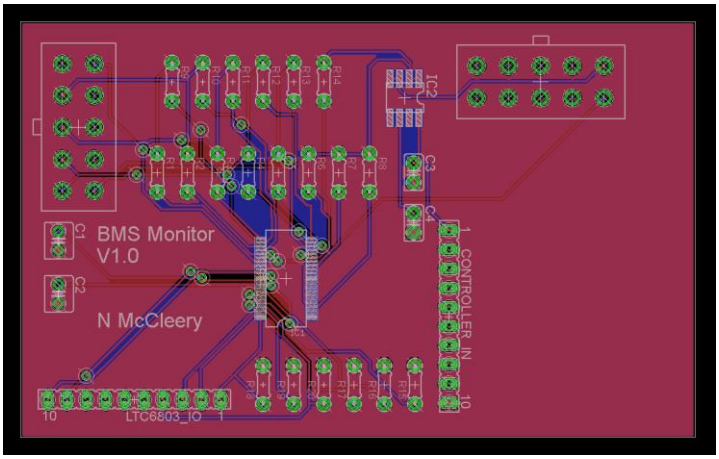

App. F - Figure 3 - PCB Layout

Note that there is no variation in PCB track width indicated in **Error! Reference source not found.**. However, when board specification (i.e. copper thickness and conductivity) information becomes available, it will be possible to adjust track widths based on required current handling and permissible temperature increase due to Joule heating.